applied sciences

MDPI

Review

A Review of Hydrogen Sensors for ECLSS: Fundamentals, Recent Advances, and Challenges

Chenghao Jia [1,2], Ling Zhao [1], Gang Huang [1,3], Litao Liu [1,3], Weirong Wang [1], Yunkai Yang [1] and Yang Miao [2,4,*]

[1] China Astronaut Research and Training Center, Beijing 100094, China; jch15239599035@163.com (C.J.); zhaodou1984@163.com (L.Z.); huanggang1971@sina.com (G.H.); tsinghuatao@163.com (L.L.); wwr507@163.com (W.W.); yang_yunkai@163.com (Y.Y.)
[2] Faculty of Materials and Manufacturing, Beijing University of Technology, Beijing 100124, China
[3] National Key Laboratory of Human Factors Engineering, China Astronaut Research and Training Center, Beijing 100094, China
[4] Beijing Key Laboratory of Advanced Manufacturing Technology, Beijing University of Technology, Beijing 100124, China
* Correspondence: miaoyang@vip.126.com

Abstract: The development of hydrogen sensors with high detection accuracy, fast response times, long calibration periods, and good stability has become the focus of the space station environmental control and life support subsystem. We analyze the current research status of different types of hydrogen sensors, including catalyst combustion type, heat conduction type, semiconductor type, fiber optic type, etc. The response signals of most hydrogen sensors are affected by temperature and humidity, resulting in cross-sensitivity. Reducing the cross-sensitivity of temperature, humidity, and other interfering factors to achieve accurate hydrogen measurement in different environments is a challenge that limits the development of hydrogen sensors. Several hydrogen sensors that are currently commercially available have a narrow operating temperature range, most of them can only measure at room temperature, and high-temperature environments require a higher accuracy and lifetime of the sensor than required at room temperature. Many new hydrogen-sensitive materials were developed to improve the performance of the sensors. The excellent performance of fiber-optic hydrogen sensors is beneficial to temperature compensation and distributed multiparameter measurement, as well as to the research and development of intelligent sensing systems, in the context of the Internet of Things. The signal detection and demodulation techniques of fiber-optic sensors are the focus of future hydrogen sensor research.

Keywords: hydrogen energy; sensor; sensitive materials; detecting technology

check for updates

Citation: Jia, C.; Zhao, L.; Huang, G.; Liu, L.; Wang, W.; Yang, Y.; Miao, Y. A Review of Hydrogen Sensors for ECLSS: Fundamentals, Recent Advances, and Challenges. *Appl. Sci.* **2023**, *13*, 6869. https://doi.org/10.3390/app13126869

Received: 26 April 2023
Revised: 19 May 2023
Accepted: 31 May 2023
Published: 6 June 2023

Copyright: © 2023 by the authors. Licensee MDPI, Basel, Switzerland. This article is an open access article distributed under the terms and conditions of the Creative Commons Attribution (CC BY) license (https://creativecommons.org/licenses/by/4.0/).

1. Introduction

The manned space station environmental control and life support system (ECLSS) is the infrastructure required to guarantee the survival of astronauts in the complex and changing space environment. Since astronauts in manned space stations are mostly in orbit for medium-to-long periods, the space station is equipped with a semi-regenerative environmental control and life support system, i.e., a physical–chemical regeneration system. The physical–chemical regenerative life technology remains the primary life support technology used on the space station today and will be so for a long time to come. This technology produces oxygen via electrolysis of water to meet the breathing needs of astronauts during their life on the space station and as a means of controlling the partial pressure of oxygen in the sealed module atmosphere. The hydrogen, as a product of the electrolytic oxygen production, is eventually discharged to the bunker or supplied to the CO_2 reduction system as a feedstock for the CO_2 reduction reaction. However, hydrogen is very permeable and is highly susceptible to leakage during system operation, and will explode when the hydrogen content in the air reaches 4–74.4% if it encounters an open flame.

The lack of timely and effective means of hydrogen monitoring will seriously threaten both astronauts' lives and the safety of manned spacecraft cabin equipment. The hydrogen sensor is a sensing device that detects the concentration of hydrogen and generates a response signal, which has the advantages of small size, low cost, online measurement, and short response time compared to traditional detection instruments [1–6]. Therefore, the development of hydrogen sensors with a high detection accuracy, a fast response time, a long calibration period, and good stability has become the focus of regenerative life support technology design.

According to the principle, hydrogen sensors can be divided into catalyst combustion type [7–9], heat conduction type [10–12], semiconductor type [13–15], fiber-optic type [16–18], etc. Currently, hydrogen sensors of the heat conduction principle are used for hydrogen concentration detection in the electrolytic oxygen generation system of the space station, and hydrogen sensors of the catalyst combustion principle are used for hydrogen concentration detection in the space station environment. The purpose of this paper is to describe and review the working principles and characteristics of the catalyst combustion and heat conduction type hydrogen sensors based on the practical application requirements of hydrogen sensors for space stations' physical and chemical regeneration systems. The article also provides a preliminary summary of the operating principles and characteristics of semiconductor-type and fiber-optic-type hydrogen sensors. Finally, recent technological developments and performance improvements in hydrogen sensors are reviewed, and the future of hydrogen sensors is discussed.

2. Catalyst Combustion Hydrogen Sensors

Hydrogen sensors based on the catalyst combustion principle became a research hotspot in hydrogen measurement technology due to their good stability and high sensitivity, and are widely used in the aerospace field [19–21]. The catalyst used in this type of sensor is metallic Palladium (Pd), which has two disadvantages. Firstly, the reaction temperature is high, and the catalyst needs to be heated, while the reaction temperature is as high as 500 degrees, and the product has high power consumption. Secondly, it is susceptible to humidity, and long-term operation under certain conditions can lead to phenomena such as agglomeration of catalyst grains, resulting in changes in the catalytic capacity of the catalyst and causing drift in the sensor output. In recent years, domestic and international research on the catalyst combustion principle of hydrogen sensors focused on the modification and preparation of catalyst materials to complement the two inherent disadvantages of the current conventional catalysts, which are high reaction temperature and interference by humidity [22,23].

2.1. Principle of Concentration Measurement

The structure schematic of the catalyst combustion-type hydrogen sensor is shown in Figure 1. It consists of a sensitive element and a compensation element, in which the pill-beaded sphere is its sensitive body, and the sensitive body of the sensitive element contains a catalyst. The sensitive body of the compensation element contains no catalyst and is used to compensate for the effect of ambient temperature changes on the hydrogen sensor output. The working principle of the catalyst combustion-type hydrogen sensor is that hydrogen reacts with oxygen on the surface of the catalytic sensor to release heat. Using a sensitive element, a compensating element, and a fixed resistor to form a bridge, the heat generated via the catalytic combustion of the combustible gas is conducted to the wrapped platinum (Pt) coil, causing the resistance of the coil to rise and, thus, causing a change in voltage in the bridge path of the sensing signal. This principle can be used to detect any combustible gas, including hydrogen.

When the hydrogen sensor works normally, the Pt wire of the sensor itself generates heat under the condition of applied voltage, meaning that the temperature of the sensitive body ranges from 200 to 300 °C. In this temperature range, a certain volume fraction of hydrogen reacts with oxygen in the air under the action of a catalyst, and the reaction

heat is generated, meaning that the resistance value increases accordingly. In general, the volume fraction of hydrogen in the atmosphere that is measured is not too high, i.e., below 4%, and the hydrogen can be burned completely, with its heat generation being related to the volume fraction. The larger the volume fraction of hydrogen in the environment that is measured, the greater the heat of the reaction, the greater the temperature increase in the platinum wire, and the greater the increase in its resistance value. Therefore, the volume fraction of hydrogen in the air can be detected via measuring the change in resistance of the Pt wire ΔR. The bridge circuit of the catalyst combustion-type hydrogen sensor is shown in Figure 2, where F1 is the sensitive element and F2 is the compensation element. When F1 is in contact with hydrogen, heat is released due to violent oxidation, which causes the temperature of F1 to rise and the resistance value to increase accordingly.

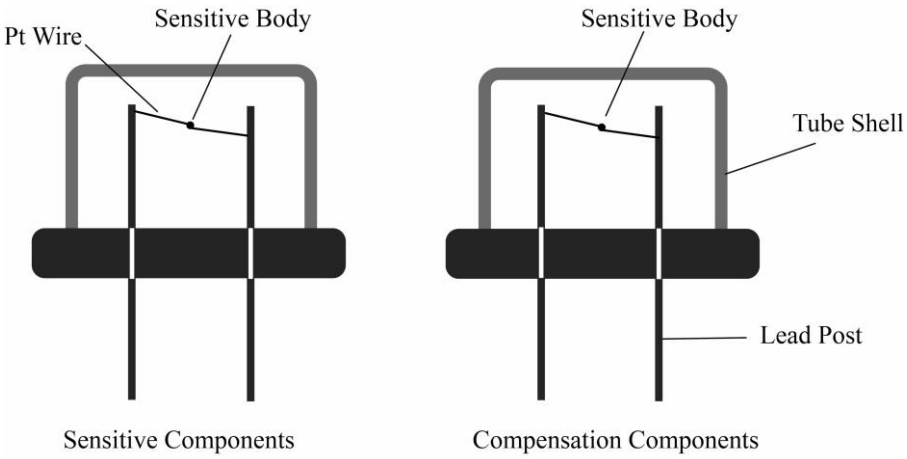

Figure 1. Schematic diagram of structure of catalytic combustion hydrogen sensor.

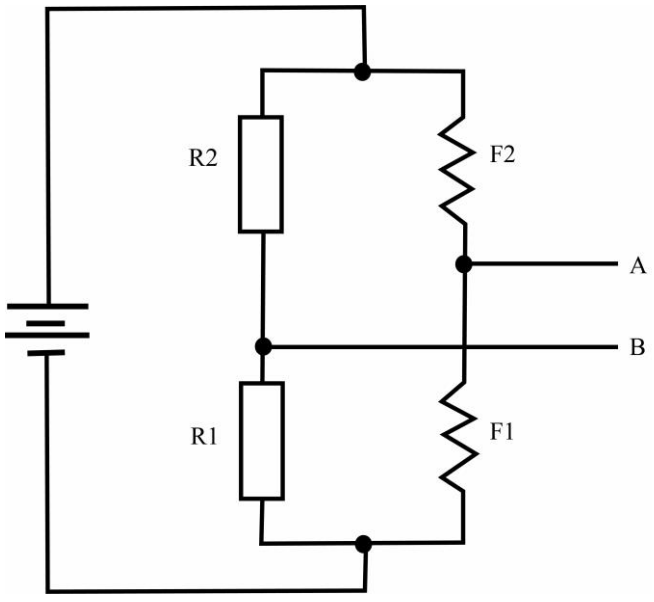

Figure 2. Bridge circuit diagram of thermoelectric catalytic hydrogen sensor.

The bridge circuit is no longer balanced, and a potential difference E is generated between A and B. Next, there is

$$E = k(R_{F2}/R_{F2})\Delta R_F \quad (1)$$

where ΔR_F is the rate of change in the resistance of the sensitive element, and k is a constant related to the applied voltage. The potential difference E between points A and B is

approximately proportional to ΔR_F in the range where the resistance ratio R_{F2}/R_{F1} of the compensating element $F2$ and the sensitive element $F1$ is close to 1. Moreover, ΔR_F is due to the heat of combustion released via hydrogen combustion, which is proportional to the heat of combustion and can be expressed using Equation (2)

$$\Delta R_F = \alpha \Delta T = \alpha(\Delta H/C) = \alpha \cdot a \cdot m(Q/C) \quad (2)$$

where α is the resistance temperature coefficient of the sensitive element, ΔT is the value of temperature increase generated via hydrogen combustion, ΔH is the heat generated via the catalytic combustion of hydrogen, C is the heat capacity of the sensitive element, Q is the heat of combustion of hydrogen, a is the volume fraction of hydrogen, and a is the constant determined via the catalyst on the sensitive element. The values of α, C and, a are related to the material, shape, and surface treatment of the sensitive element. Q is a certain value, if we make $K = ka\alpha Q/C$, and K is a constant value under certain conditions. Thus, we have

$$E = Km \quad (3)$$

That is, the potential difference between points A and B is proportional to the volume fraction m of the combustible gas. If a voltmeter is connected between points A and B, the potential difference E between points A and B can be measured, and the volume fraction of flammable gas in the air can be found.

2.2. Status of Research

Catalyst combustion sensors have a long history. The first catalyst combustion sensor was proposed by Jones in 1923 using a bare Pt wire and was first used for methane detection in mines [24]. The bare Pt wire sensing element is simple in structure, easy to make, and highly resistant to toxicity. However, due to the high operating temperature, the service life was greatly reduced. To further improve the performance of catalytic sensors, Baker first introduced the concept of pellistor in 1959 using a carrier and catalyst coated into a Pt wire ring to prepare a catalytic sensor [25]. This catalytic element usually uses a metal Pt with a diameter of 10 to 50 μm that is embedded into a metal Pd catalyst with a refractory material as a carrier. As catalytic combustion proceeds, the temperature rises, leading to an increase in the resistance of the Pt wire, which is then output as a signal. Although many researchers subsequently used research to improve the sensing performance, the structure and catalytic principle of catalytic combustion-type sensors have not changed significantly and have been applied until today. With the development of science and technology, researchers worked to improve the sensitivity, reduce power consumption, and miniaturize the catalytic element mainly through optimizing the sensor components and improving the preparation of catalysts. Houlet et al. [26] proposed a miniature thermoelectric catalytic hydrogen sensor, which consists of a thermopile of 18 thermocouples on an insulating thin film. The thermocouples convert the catalytic combustion heat into voltage and current signals output, with their output voltage being 11 times higher than that of a single thermocouple sensor, while the thermoelectric power is 15 times higher. Krebs et al. [27] fabricated an integrated catalytic combustion-type sensor for the detection of combustible gases using a thin film deposition technique. The sensor has very low power, typically only 100 mW, and an operating temperature of 400 °C. Kim et al. [28] prepared thin-film micro hydrogen sensors via sol-gel synthesis of SnO_2-Ag_2O-PtOx composites loaded on alumina substrates, which exhibited high selectivity and fast response. Henriquez et al. [29] synthesized hollow microrod-like Pt nanostructures on a small suspended microheater platform. As the catalytic layer of the low-power thermoelectric catalytic hydrogen sensor, the hydrogen collides locally on the surface of the Pt nanostructures during operation and transfers heat to the microheater, thus changing its resistance. The sensor exhibits high sensitivity, fast response, and low power consumption. Ivanov et al. [30] studied several platinum group catalysts and discussed the sensitivity and temperature dependence of the sensors. It was found that the use of Iridium and Rhodium as catalysts could

effectively improve the low-temperature performance of hydrogen sensors with Pd and Pt as catalysts. Some scholars also attempted to use nanostructures or new materials, such as graphene, for catalyst surface modification, which was performed to improve the sensitivity and detection range of thermoelectric catalytic hydrogen sensors [31,32]. For example, Pujadó et al. [33] developed a sensor based on functionalized thermoelectric silicon nanotubes with a detection limit of 250 ppm at room temperature, and the response signal and hydrogen concentration remained well linear over a wide range.

Catalytic hydrogen sensors have the advantages of fast response times, long lives, and high accuracy. The technology is now mature and commercially available. However, the gas selectivity of these sensors is poor, and they must be used in the presence of oxygen to achieve measurements. In addition, the catalytic hydrogen sensor will release a lot of heat during operation, which may cause the risk of ignition or explosion.

3. Heat Conduction Hydrogen Sensors

As the thermal conductivity of each gas is different, with the change in the concentration of the measured gas, the thermal conductivity of the thermistor on the thermal conductivity core to the measured gas is different, and the temperature of the sense resistor on the thermal conductivity core changes, which finally leads to the change in the resistance value of the sense resistor on the thermal conductivity core. There will be no chemical reaction, let alone material change; thus, its output is very stable and the drift is very small in long-term use, which can meet the actual application requirements in the aerospace field.

3.1. Principle of Concentration Measurement

The heat conduction-type hydrogen sensor belongs to the crossover class of electrical and physical thermodynamics sensors; its detection circuit is based on the design theory of a balanced bridge, while its detection principle is based on thermodynamics [34–38]. Figure 3 shows a heat conduction-type hydrogen sensor, which is designed based on the theory that each gas has a different thermal conductivity. Its most important feature is the constant temperature measurement, which is determined via the current flowing through the thermal material. The thermal material is usually a Pt wire with good thermal conductivity. When the target gas flows through the Pt wire, some of the heat from the wire is transferred to the gas. For different concentrations of the same gas and two gases with different levels of thermal conductivity, the amount of heat transferred in the process is not the same. The heat transferred is, therefore, a reflection of the type and concentration of the target gas. In the detection circuit, a balanced bridge design is used, in which the thermal element is used as one of the measuring bridge arms. The loss of heat from the Pt wire causes a change in its temperature, the balance of the bridge is broken at the initial operating current, and the bridge outputs a differential pressure signal to the outside. After the two processes of heat conduction and conversion of the bridge, the amount of heat transferred is converted into the size of the output voltage signal. Therefore, by measuring the differential voltage signal of the bridge, the concentration of the target gas can be reflected.

The concentration detection is achieved by relying on a Wheatstone bridge built with a Pt wire resistor and divided into a measurement arm and a reference arm. A reference gas is encapsulated in the reference arm, which is designed to weaken the effect of ambient temperature changes on the bridge. When the measured gas flows through the measuring arm, the temperature of the Pt wire of the measuring arm changes, and the bridge loses its balance and outputs a voltage difference signal. Once the composition of the target gas is determined, its thermal conductivity only changes with gas concentration.

To make the heat conduction-type sensor work stably, a thermostatic circuit is needed to ensure that the detector works properly. Figure 4 shows the principle circuit for thermostatic detection of heat conduction-type gas sensors. Resistors R_1, R_2, R_3, and r form a Wheatstone bridge to convert the unbalanced voltage output. Here, R_2 and R_3 form the reference bridge arm, R_1, while r forms the measurement bridge arm and is the heat conduction-type sensor. When the target gas concentration in the environment is 0, the

bridge is in equilibrium, i.e., $R_2R_3 = rR_1$. The operating current of the sensor is reasonably adjusted to provide a constant temperature for the normal operation of the sensor. When the target gas detection is carried out, as the thermal conductivity of the target gas increases, the temperature of the thermal conductivity sensor decreases, causing its resistance to decrease and breaking the equilibrium of the original bridge. The signal output outputs an unbalanced voltage u_0, and after differential amplification and subsequent circuit processing, the value of u_0 can be measured to detect the concentration of the target gas. When the gas concentration becomes 0, the bridge also restores the balance; thus, the resistance of the sensor and the temperature remain unchanged, which is regarded as constant temperature detection.

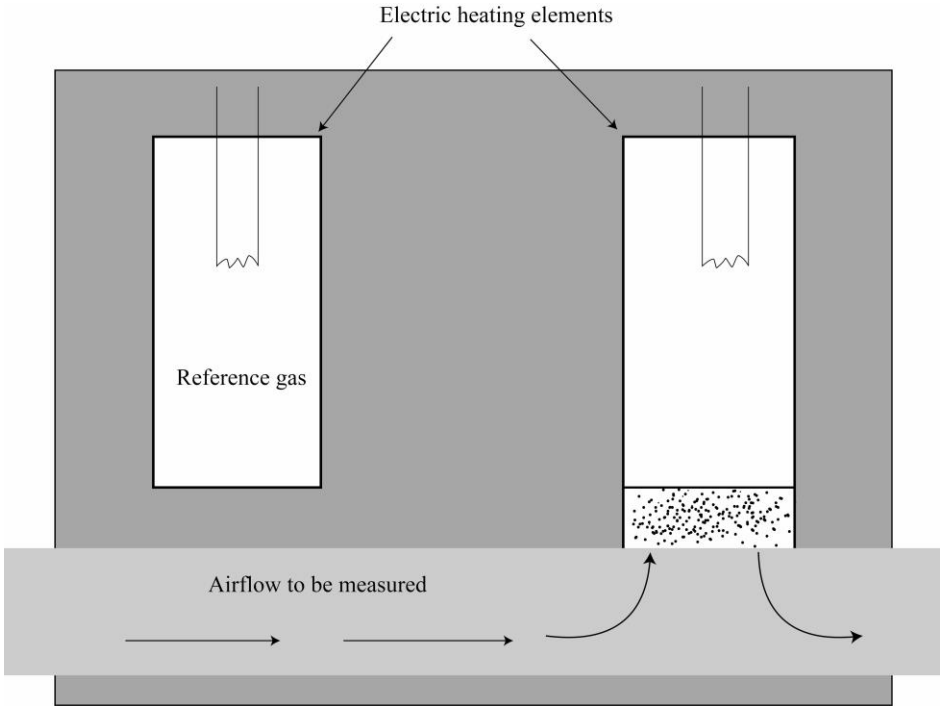

Figure 3. A type of heat conduction hydrogen sensor.

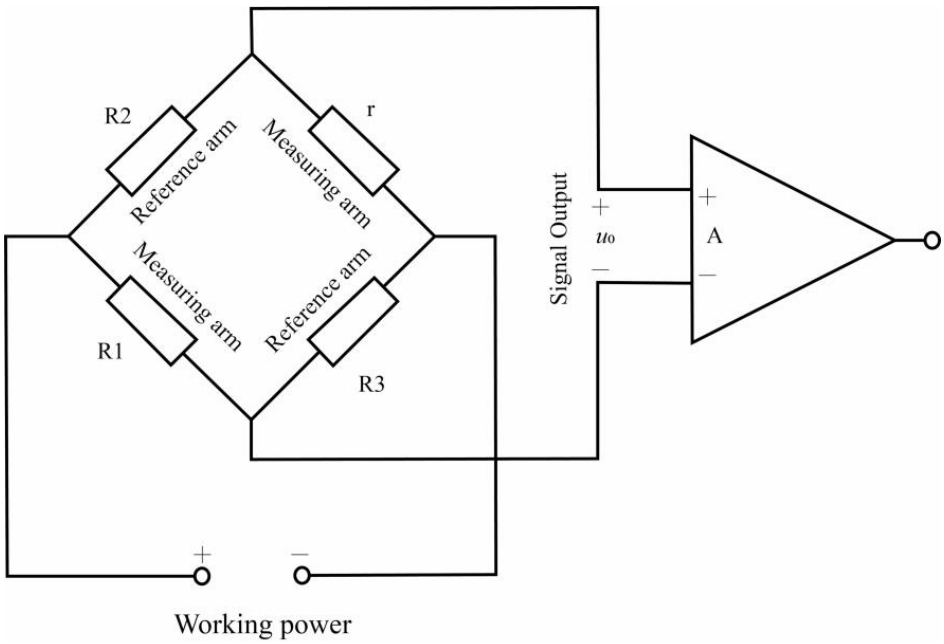

Figure 4. Heat conduction-type hydrogen sensor detection circuit.

A quantitative analysis of the thermostatic detection principle of the heat conduction-type gas sensor is herein carried out. We assume that the operating current of the sensor is I and the internal resistance is r. Ideally, all the heat of the sensor is generated via the internal resistance in the rated state, i.e., $Q_i = I^2 r$. It is known from physics that there are three cases of heat transfer: heat conduction, heat radiation, and heat convection. The length of the selected detection element resistive wire is often much larger than its diameter, meaning the heat loss in the axial direction can be ignored. Considering also that heat convection does not exist in practical applications, the heat loss is, therefore, composed of only two parts: heat conduction loss of heat Q_1 and heat radiation loss of heat Q_2.

$$Q_0 = Q_1 + Q_2 \tag{4}$$

where the expression for Q_1 is

$$Q_1 = \lambda S(T - T_0) \tag{5}$$

the thermal conductivity of the gas is λ, the sensor temperature is T, the ambient temperature is T_0, both Ts are Kelvin temperatures, and the surface area of the sensor is S. According to Stephen Boltzmann's law, the expression for Q_2 is

$$Q_2 = A\sigma S\left(T^4 - T_0^4\right) \tag{6}$$

the radiation coefficient is A, while σ is the Stephen Boltzmann constant. According to the law of conservation of energy, the heat produced is dynamically balanced with the heat lost; therefore,

$$Q_i = Q_0 = Q_1 + Q_2 \tag{7}$$

$$I^2 r = \lambda S(T - T_0) + A\sigma S(T - T_0) \tag{8}$$

When the target gas concentration is 0, the Wheatstone bridge is in equilibrium and the initial operating current of the sensor is I_0. The thermal equilibrium equation at this point is

$$I_0^2\, r = \lambda_0 S(T - T_0) + A\sigma S(T - T_0) \tag{9}$$

When the target gas measurement is carried out, the thermal conductivity of the target gas mixed with air is λ_1; the ambient temperature T_0 is kept constant; the sensor is detected at a constant temperature, meaning that the temperature T is also kept constant; and the initial current I_0 is transformed into the operating current I. The above equation can be combined to obtain the constant temperature detection equation of the sensor:

$$I^2 = I_0^2 + \frac{(\lambda_1 - \lambda_0)S(T - T_0)}{r} \tag{10}$$

From the above equation, it can be seen that, in practice, r, T_0, T, S, λ_0, and I_0 are definite values; thus, $I_2 \propto \lambda_1$. The difference between the set operating current and the initial test circuit is ΔI.

$$I = I_0 + \Delta I \tag{11}$$

Substituting Equation (10) into Equation (9), while ignoring the small change ΔI, it is true that

$$\Delta I = I_0 + \frac{(\lambda_1 - \lambda_0)S(T - T_0)}{2I_0 r} \tag{12}$$

From this equation, it can be seen that the current I is linearly related to the thermal conductivity λ_1 of the target gas when ΔI does not change much. Next, using Ohm's law, this operating current flows through the resistor and becomes a potential signal output, which represents the change in the thermal conductivity of the gas mixture. According to the thermodynamic knowledge, when the target gas is in the background gas of air, the

λ_1 of the gas mixture is linearly related to the concentration C of the target gas, and the expression is

$$C = \frac{\lambda_1 - \lambda_0}{\lambda - \lambda_0} \quad (13)$$

Therefore, it is only necessary to know the thermal conductivity λ_1 of the gas mixture to obtain the concentration C of the target gas and complete the measurement of the gas concentration.

3.2. Status of Research

Thermally conductive hydrogen-sensitive materials include not only the precious metals Pt and Pd, which play a catalytic role, but also thermoelectric materials, which convert a temperature difference into electrical signals. Masahiko et al. [39] showed that the catalytic activity of Pt film increases with the increase in film thickness, and when the film thickness exceeds 60 nm, the catalytic activity of Pt film reaches saturation and no longer increases with the increase in film thickness. In addition, the smaller the Pt particle size, the better the catalytic activity of Pt film, and when the film thickness exceeds 150 nm, the catalytic activity of Pt film is no longer affected by Pt particle size. Recently, Y. Choi et al. [40] showed that the catalytic activity of powdered catalysts is higher than that of thin film-type catalysts because the powdered material has a larger specific surface area and roughness, which is more tolerant to contact with hydrogen. They developed a micro-thermal heat conduction-type hydrogen sensor using a mixture of Pt and Al_2O_3 powders as catalysts, which can detect hydrogen in the concentration range of 0.005–3% at room temperature, and found that the catalyst activity was maximum when the mass ratio of Pt and Al_2O_3 was 2:3. Thermoelectric materials require a small heat capacity and fast heat transfer. W. Shin et al. [41] developed a heat conduction-type hydrogen sensor by plating a Pt catalytic film on the 1/2 surface of NiO film, which can detect hydrogen in air at 0.025–10% concentration. Here, there is a good linear relationship between the detection signal and hydrogen concentration, and the films can quantitatively detect a higher concentration of hydrogen when nitrogen is used as the dilution gas. The conductivity of thermoelectric materials can be controlled via basic doping, such as Li, Na, Ni, etc. Qiu et al. [42] reported that a Ni film (30 nm) was sputtered on a SiGe film (3 μm), and after annealing at 500–600 °C, the SiGe was transformed from an amorphous to a crystalline state. A Pt film (1 μm) was then sputtered on the crystalline film to make a heat conduction-type hydrogen sensor. The research shows that the crystallinity of the thermoelectric material has a great influence on the hydrogen-sensitive performance of the element, and the greater the crystallinity, the better the hydrogen-sensitive performance.

The design of the heat conduction-type hydrogen sensor is based on the theory that the thermal conductivity of hydrogen is greater. In a gas mixture including air, the thermal conductivity of oxygen is less than one-eighth that of hydrogen; thus, the thermal conductivity of the gas mixture is mainly determined based on the concentration of hydrogen. Heat conduction-type sensors are currently used in many applications due to their large measuring range, variety of gases measured, and high stability. At the same time, heat conduction-type gas sensors also have technical advantages, such as long life, good stability in a large detection range, and low cost. However, because the thermal conductivity sensor detects the concentration based on the temperature change in the thermal element, the measurement results will be affected to some extent by the selection of gas-sensitive materials and thermal conductivity, resulting in low accuracy, low sensitivity, large temperature drift, and other problems. To solve the problems of thermal conductivity gas sensors, their detection methods must be improved to overcome the defects of temperature drift [43–46].

4. Semiconductor Hydrogen Sensors

When the sensor is exposed to hydrogen, the adsorption and permeation of hydrogen change the resistance of the hydrogen-sensitive material in the sensor, and the resistance of the hydrogen-sensitive material changes again when the hydrogen is removed from the

hydrogen-sensitive material. There are two main types of semiconductor-type hydrogen sensors: metal oxide- and non-resistive-type sensors (i.e., metal or alloy type).

4.1. Metal Oxide Semiconductor Hydrogen-Sensitive Materials and Sensors

The metal oxide-type hydrogen sensor includes a metal oxide layer with semiconductor characteristics that is deposited on a heater, thereby raising the temperature of the layer to an operating temperature (500 °C). The principle of operation is that when oxygen from the environment is adsorbed in the metal oxide layer, which has a high resistivity when hydrogen diffuses into the sensing layer and reacts with oxygen, it is adsorbed on the surface of the semiconductor metal oxide and the resistivity of the adsorbed layer decreases, while the value of the decrease increases with the increase in the concentration of hydrogen (see Figure 5). The semiconductor metal oxide-type hydrogen sensor has the advantages of simple structure, cheap price, high sensitivity, fast response, and easy compounding; thus, it is conducive to mass production [47].

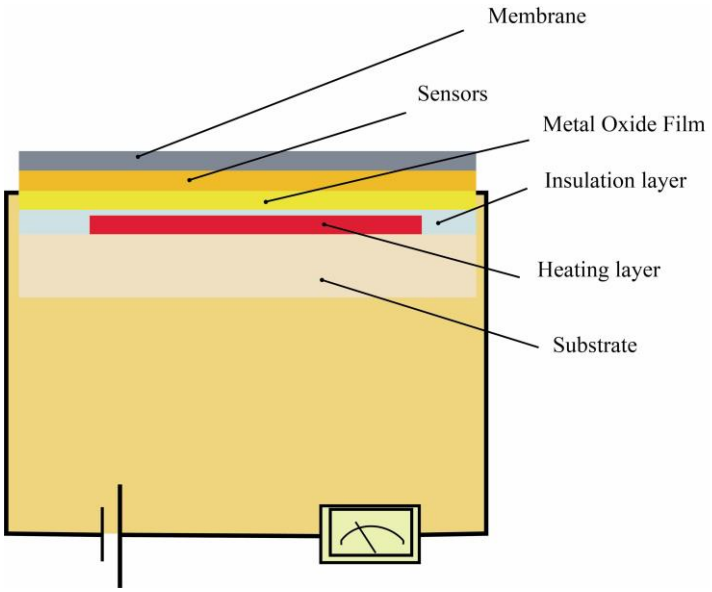

Figure 5. Schematic diagram of metal oxide semiconductor-type hydrogen sensor structure.

Most metal oxide semiconductor-type hydrogen sensors are highly sensitive, with average response times being between 4 and 20 s. However, the poor response speed of a single metal oxide makes it difficult to meet practical needs. Moreover, the single metal oxide has poor selectivity to hydrogen, lacks sensitivity to hydrogen, and is highly susceptible to interference from other reducing gases, such as CO, CH4, alcohol, etc. To improve their selectivity, this problem can be solved via doping with noble metals with good selectivity for hydrogen, such as Pt, Pd, Au, etc. Rashid et al. [48] presented a method for hydrogen detection at room temperature using ZnO nanorods doped with a Pd catalyst. Pd nanoparticles with a size of about 10 nm were used as catalysts and deposited into the ZnO nanorod array network via RF magnetron sputtering to detect hydrogen concentration in the range of 0.2 to 1000 ppm at room temperature with fast response and stable performance. Mirzaei et al. [49] reviewed the research work on improving the performance of resistive hydrogen sensors using Pd. However, precious metals are costly and sensitive to chemicals such as sulfur-containing substances and CO. To overcome these drawbacks, it was shown that transition metal dopants, such as zinc, manganese, cobalt, and copper, have significant effects in improving metal oxide sensors. The selectivity, optimum operating temperature, and response/recovery time of the sensors were improved [50]. In addition, doping with rare earth elements can also significantly enhance the sensor response [51]. In addition to metal oxides, semiconductor materials include sulfides, nitrides, etc. Gottam et al. [52] presented a highly sensitive hydrogen sensor that used

MoS_2-Pt nanoparticle films as the active layer. For 100 ppm H_2, the sensor achieved ultra-fast response and recovery rates of 4 s and 19 s, respectively. When exposed to 100 ppm H_2, the MoS_2-Pt composite film exhibited a high sensor response, which was superior to existing metal sulfide-based sensors. Hermawan et al. [53] studied a GaN hydrogen sensor. The GaN hydrogen sensor exhibited high stability and sensitivity under a high-temperature environment. Hermawan et al. [54] studied a wide band gap aluminum nitride (AlN) sensor material, which can withstand high-temperature environments. Three unique AlN morphologies (rod, nested, and hexagonal plate) were synthesized via direct nitridation at 1400 °C using γ-AlOOH as a precursor. The gas-sensing performance showed that the hexagonal plate form exhibited good reproducibility and the highest response to 750 ppm H_2 leakage at high temperature (500 °C) compared to the rod and nested forms.

4.2. Schottky Diode Hydrogen-Sensitive Materials and Sensors

Non-resistive semiconductor hydrogen sensors sense hydrogen according to the response of the potential barrier and capacitance of the material about the hydrogen concentration. Depending on the principle and structure, they can be divided into Schottky diode-type and metal oxide semiconductor-type field-effect transistors (MOSFET). As shown in Figure 6, Schottky diode-type hydrogen sensors generally deposit a layer of metal (usually Pd or Pt) on the semiconductor material to form a Schottky junction. A metal oxide insulating layer is also usually added between the two components to improve the stability and sensitivity of the sensor to hydrogen. When the metal comes into contact with hydrogen, the hydrogen molecules decompose into hydrogen atoms and diffuse into the semiconductor layer, causing a change in the Schottky barrier, and the hydrogen concentration is detected through detecting current or voltage. Ajayan et al. [55] and Irokawa et al. [56] reviewed Schottky diode-type hydrogen sensors using nitride-based semiconductor materials, with GaN and AlGaN showing better performance with very high sensitivity and fast response times, respectively. The sensing signal of the GaN hydrogen sensor is affected by the ambient temperature, and Baik et al. [57] introduced a reference diode to compensate for the temperature of the GaN hydrogen sensor.

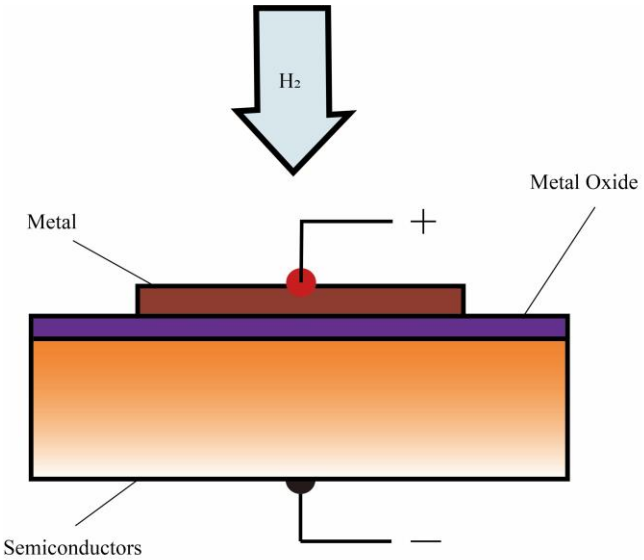

Figure 6. Schematic diagram of Schottky diode hydrogen sensor structure.

The advantages of semiconductor-type hydrogen sensors are their simple structure, small size, easy integration, low cost, fast response, and suitability for mass production. However, they are affected by electromagnetic interference and are prone to signal drift, making them difficult to use in harsher environmental conditions. In addition, sparks may be generated, while there are combustion, explosion, and other safety issues.

5. Fiber-Optic Hydrogen Sensors

With the recent development of optical testing technology and fiber-optic communication technology, optical sensing technology, which uses optical fibers as a carrier to sense and transmit environmental parameters through light wave signals, was also applied to hydrogen concentration detection, which can also be generally referred to as fiber-optic type sensors [58–61]. Catalytic and electrical hydrogen sensors can respond quickly and accurately to hydrogen concentration at room temperature and pressure and are currently used in; however, these sensors, which are based on electrical characteristics, may generate sparks during use and have the potential to cause hydrogen explosions, which are a safety hazard. Fiber-optic sensors detect hydrogen through sensitive materials and optical signals, which are intrinsically safe and immune to electromagnetic interference, and have the advantages of small size, wide measurement range, and resistance to high temperatures and pressures. Fiber-optic hydrogen sensors are divided into interference modulation type, intensity modulation type, and wavelength modulation type.

5.1. Interference-Modulated Fiber-Optic Sensors

In 1984, Butler et al. [62] developed the first interferometric fiber-optic sensor for hydrogen leak detection. The sensor optical path structure is shown in Figure 7, being similar to the Mach–Zehnder fiber interferometer. The optical path consists of two single-mode fibers, both of which are stripped of the same length (3 cm) of cladding and coated with different material films at the stripped location. One of the fibers was sputtered with a 10 nm thick Ti film, followed by a 10 μm thick Pd film. The Ti coating is used to increase the adhesion between the palladium and the fiber; the other fiber is sputtered with a Pt film at the corresponding location to match the response of the two fibers to temperature. The fiber with the Pd coating is used as the sensing optical path, and the fiber without the Pd coating is used as the reference optical path. To prevent the effect of mechanical vibration, the two fiber sensing sites are closely pasted on a quartz plate. The light source is a 0.5 mW He-Ne laser, and the laser beam is split and focused into the optical fiber by the lens. When the Pd film on the fiber surface encounters H_2, the Pd film expands, causing the fiber to stretch, thus changing the optical range of the transmitted light. The change in the optical range causes the movement of the interferometer interference fringe. The output of the interferometer is equipped with a photoelectric detector for detecting the number of interferometric fringe movements. The number of moving stripes is related to the H_2 concentration that is measured.

For the experiments, different carrier gases, such as argon, nitrogen, and dry air, were used. The results showed that though the response times were different for different carriers, they were all in the order of minutes. The measurement range was 10–4% (1 ppm)–3%. In 1988, researchers improved the manufacturing process of Pd film to improve measurement accuracy [63]. Figure 8 shows the variation in streak motion versus hydrogen concentration. In the figure, the right vertical dashed line is the boundary between phases and the transition phase, the straight solid line represents the theoretical value described via Sieverts' law, the curved solid line represents the theoretical value described via Langmuir's equation, and the curved dashed line is the experimentally fitted value. As can be seen from the figure, when the H_2 concentration is greater than 0.1%, the experimental value conforms to Sieverts' law, and the stripe movement in this interval is linear with the hydrogen concentration. In other words, the lattice constant increase in this interval is proportional to the hydrogen content. At lower hydrogen concentrations, the experimental results deviate more clearly from Sieverts' law, indicating that the low concentration case cannot be fully explained based on the bulk phase solubility. As the metal Pd surface is more capable of capturing hydrogen molecules at lower concentrations, more molecules are adsorbed on the Pd surface; thus, it agrees with the Langmuir equation. The sensitivity of the improved sensor reached 6–10% (20 ppm).

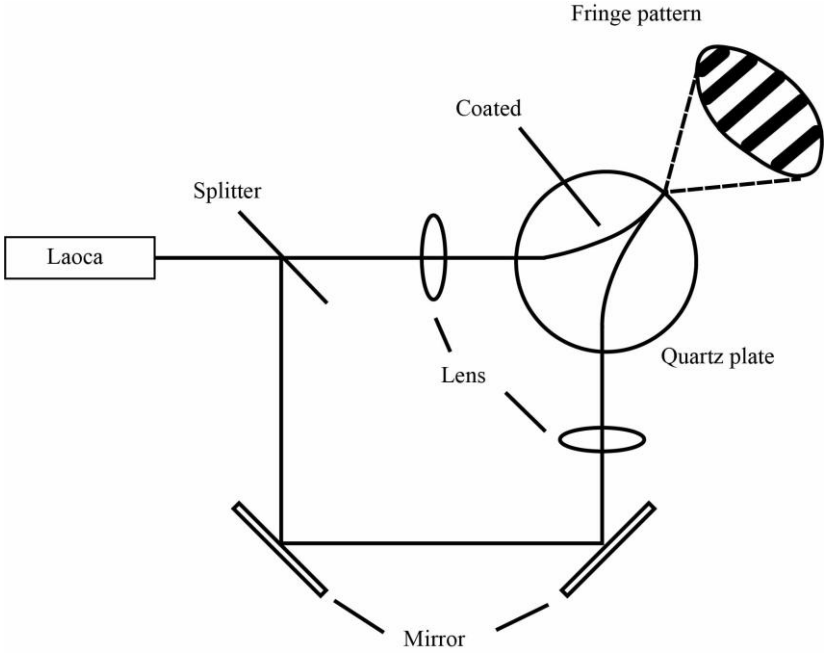

Figure 7. Butler fiber-optic-type sensor schematic.

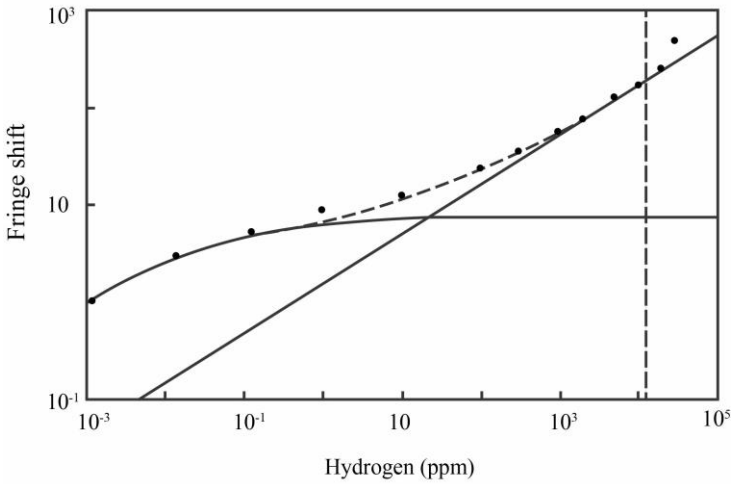

Figure 8. Interference stripes as a function of hydrogen concentration.

The hydrogenation of Pd leads to material strain, and the strain changes the optical range of the transmitted light, causing the stripe to move. In 2015, Yu C B. et al. [64] proposed an fiber-optic F-P hydrogen sensor based on Pd-Y film by measuring the streak contrast variation at different hydrogen volume fractions. The experimental results showed that the sensor has high sensitivity and the performance of the Pd-Y film is better than that of the Pd film. A 0.5 dB reduction in streak contrast was detected when the hydrogen volume fraction varied from 0 to 5.5%, and the sensor's temperature response was also measured.

Kim Y et al. [65] proposed the Sagnac interferometer fiber-optic hydrogen sensor and conducted an experimental study of the sensor performance. The reference spectra used as sensing indicators showed variations in wavelengths of 0.34, 1.51, 2.38, and 2.48 nm for hydrogen gas volume fractions of 1–4%. The response time (rise or fall time) was 10–12.5 s. The sensitivity of the sensor was improved at low hydrogen volume fraction levels due to the higher birefringence strain sensitivity of the polarization-maintaining optical fiber (PMF). The sensitivity of the sensor was improved at low hydrogen volume fraction levels.

5.2. Intensity Modulated Fiber-Optic Sensors

In 1991, Butler et al. [66] developed an intensity-modulated fiber-optic sensor. This sensor uses a miniature reflector as the sensing surface, and its structure principle is shown in Figure 9. One port of the multimode fiber is coated with a Pd film with a thickness of 10 nm and a diameter of 125 μm. The Pd film is used as a sensing surface, on one hand, and a light-reflecting surface, on the other hand, as shown in Figure 9a. The other part of the fiber is connected to a Y-shaped coupler, which is coupled to the other two fibers. One fiber is used as the input light, which is connected to the light source, and the other fiber is used as the output signal light, which is connected to the photoelectric converter. When the sensor is placed in an H_2 environment, the reflectivity R (or transmittance T) of the Pd film is changed due to the Pd-H_2 interaction, and the amount of change in reflectivity is related to the hydrogen concentration. Therefore, the amount of change in output light intensity is detected to obtain information on hydrogen concentration. Figures 9b and 10c show the variations in reflectance with time and hydrogen concentration, respectively, which were obtained experimentally. As can be seen from the figures, the reflectivity decreases with increasing concentration, and the response time varies for different concentrations. Of particular importance is the fact that the relative amount of change in reflectance in correlation with concentration is in good agreement with the P-C-T plot of Pd. This finding indicates that the relative value of the change in reflectance can be used to test the components of palladium hydride [67]. This type of sensor has the simplest structure and stable performance [68].

From the previous experimental results, it is clear that the sensing effect of microscopic mirrors depends on the extent to which the Pd-H_2 interaction affects the reflectance or transmittance of the mirrors. Kalli et al. [69] studied the optical reflectance of Pd films with thicknesses between 1 nm and 30 nm. They performed single- and multiple-repetitive adsorption/desorption for Pd films of different thicknesses to characterize the phase change process for Pd films from α-phase to β-phase for a different number of cycles. The results demonstrate that the variation in reflectance is related to various factors, such as film thickness, film structure, and substrate properties. ARMGARTH M [70] reported the effect of film surface microstructure on reflectance (or transmittance). The study selected Pd films with thicknesses ranging from 10 to 70 nm and observed that when the Pd film adsorbs H_2, molecules, microbubbles, and microcracks appear on the film surface due to the interaction between the two factors, with these two defects directly affecting the reflectivity of the film surface. They also selected thick Pd films with film thicknesses over 100 nm and found microbubbles and micro cracks on the film surface. Comparing such micro-defects in thin and thick films, the results show that micro-bubbles and micro-cracks appear in thin films after adsorption, and the defects on the film surface disappear after desorption, i.e., the defects on the film surface are reversible, while the defects in thick films are permanent mechanical damage and are irreversible. To eliminate such micro-defects, a 1–2 nm thick Ni film is plated on the fiber end face, while a Pd film is plated on top of the Ni film. The experimental results show that the reflectivity of Ni/Pd film decreases after Ni coating, and the height and width of the slowly changing reflectivity interval are different. The adhesion of Pd film to the cladding affects the microstructure of the film surface, which affects the sensing performance. The adhesion of Pd on the quartz substrate is smaller than that on the Ni substrate, and increasing the adhesion can eliminate microbubbles and micro cracks on the film surface. The study by Matelon et al. [71] shows that the nature of the substrate significantly affects the response time of the sensor. They produced a Pd/Si film with a maximum response time of 700 s, as well as a Pd/Al_2O_3 film with a maximum response time of 3700 s. They concluded that surface roughness affects the microstructure of the Pd subsurface, as well as different substrates with different surface roughness values, thus affecting the response time of the sensor. The study of optical transmittance of new metal/metal hydride thin film materials gave new impetus to the use of Pd-film sensing materials. In 2006, Kazemi et al. [72] developed an intensity fiber-optic sensor and applied the sensor to the Stennis. In 2006, Kazemi et al. [73] developed an intensity fiber-optic

sensor and applied it to the launch test of a one-time launch vehicle on Launcher IV at the Stennis Space Center. They fabricated the micro-reflector sensing surface with a porous substrate, meaning that the metal Pd could penetrate the porosity of the substrate. The porous material produced a palladium film with excellent repeatability and reliability.

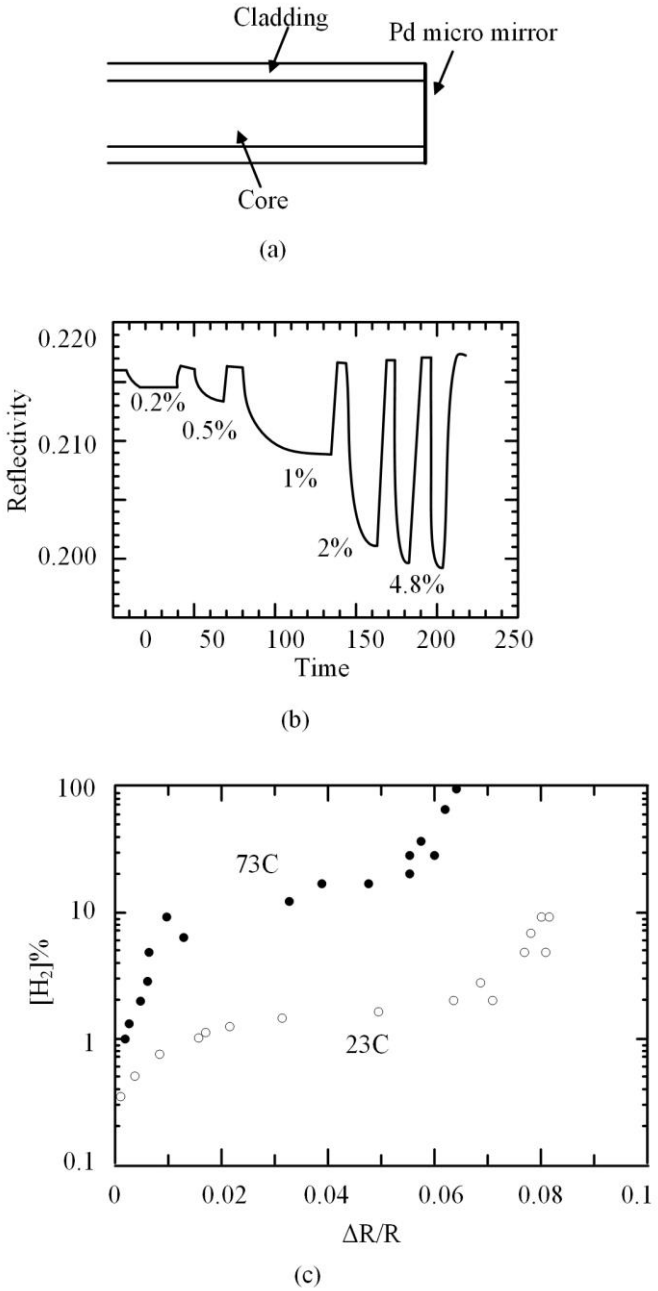

Figure 9. Micro-reflector sensing structure and test results. (**a**) Pd film effect. (**b**) Reflectance time variation relationship. (**c**) Variation of reflectivity with hydrogen concentration.

The evanescent wave type fiber-optic sensor uses a structured optical fiber with a coating on the fiber surface to achieve the measurement of hydrogen concentration using the evanescent wave effect of light waves in the light sparse medium inside the waveguide. In 1999, Tabib Azar et al. [74] developed a class of sensors based on the evanescent wave effect in optical waveguides, with the structure shown in Figure 10b. They used a multimode fiber with a core diameter of 50 μm, and the fiber was stripped of a small section (1.5 cm) of cladding and then coated with a Pd film at the stripped location with a thickness of 10 nm. A laser beam with a wavelength of 650 nm was used as the light source. The experiments

were performed with N_2 carrier gas, and the H_2 concentration varied from 0.2 to 0.6% of the sample gas. The experimental results are shown in Figure 11. The response process and the variation in signal intensity with the relative concentration of hydrogen are shown in Figure 11a,b, respectively. As can be seen from the figures, the response time of the sensor is 30 s, and the sensor can be reused with a recovery time of about 3 min. Meanwhile, the residual gas has a delay in detection of about 20 s. The transmitted light intensity increases with the concentration; however, when the concentration increases to a certain level, a saturation effect occurs.

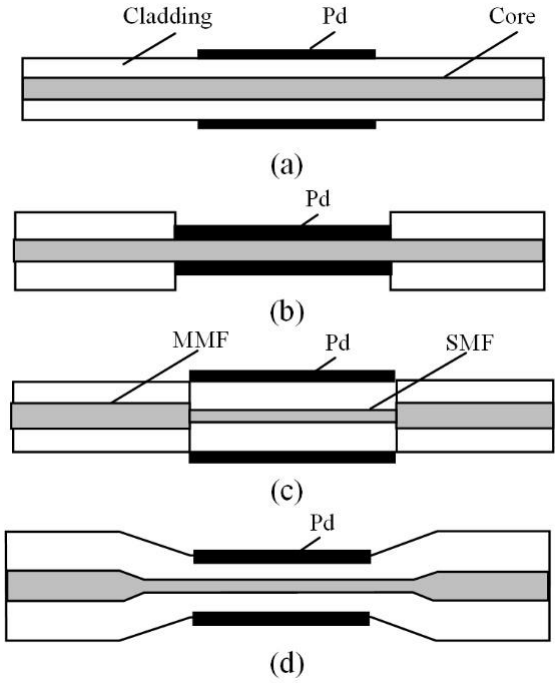

Figure 10. Schematic diagram of Tabib Azar et al.'s fiber-optic sensor. (**a**) Traditional Structure. (**b**) Traditional Structure. (**c**) Multi-film and single-film fiber coupling. (**d**) Wedge Fiber.

Physically, the Pd-H_2 interaction can cause a change in the dielectric coefficient of the material. When the imaginary part of the dielectric coefficient decreases, the light absorption coefficient of the material decreases, and the intensity of transmitted light increases. The intensity of transmitted light can be expressed as

$$I_t = I_0 \exp(-2r\Delta\alpha L) \tag{14}$$

where I_0 is the transmitted light intensity in the absence of hydrogen, r is the ratio of the evanescent wave intensity to the total intensity in the waveguide, and the magnitude of r is related to the sensor structure. Experiments show that the value of r varies widely, ranging from a few percentage points to several tens of percentage points. L is the interaction length (length of the Pd film) and A is the amount of variation in the absorption coefficient of the Pd film. Of course, with this type of sensor, the Pd-H_2 interaction not only causes a change in the imaginary part of the dielectric coefficient, but also a change in the real part of the dielectric coefficient. The change in the real part of the dielectric coefficient leads to a change in the transmitted light phase.

Several similar Tabib Azar fiber-optic sensors are also given in Figure 10, the first two of which have the simplest structure, while the last two are slightly more complex. Figure 10c uses multi- and single-mode fiber coupling, as shown in Figure 10d with wedge fiber. The sensing principle can also be understood in terms of numerical aperture variation for sensors of this type of structure. Due to the Pd-H_2 interaction, the numerical aperture of the fiber is changed, which, in turn, leads to a change in the intensity of the transmitted light.

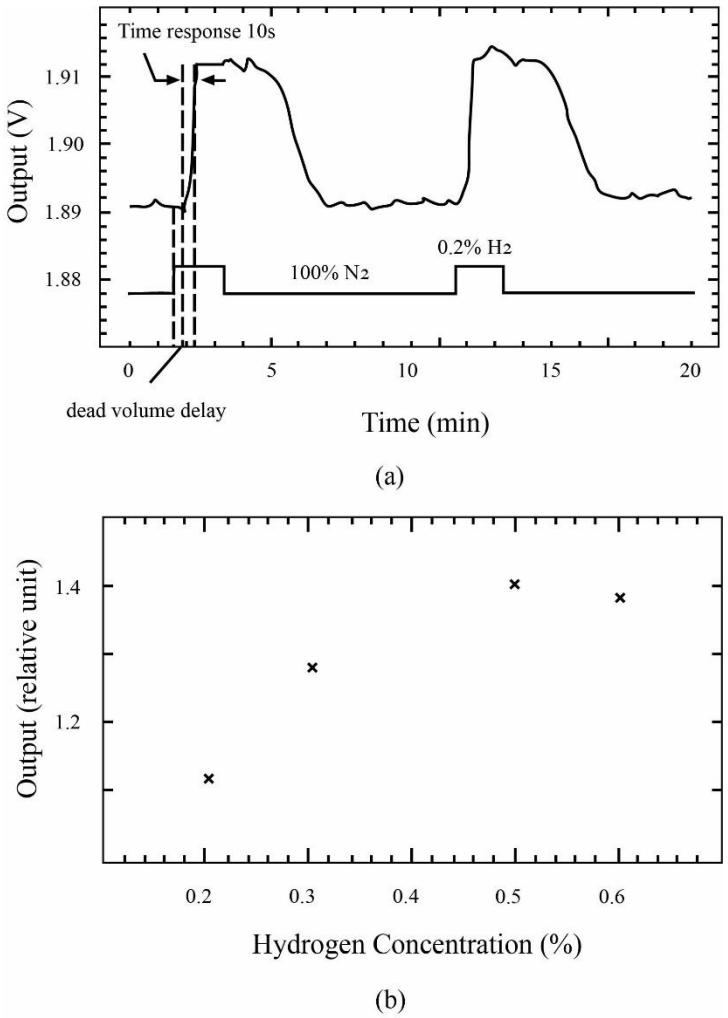

Figure 11. Experimental results of Tabib Azar et al.'s sensor. (**a**) Variation of response process with hydrogen concentration. (**b**) Variation of signal intensity with hydrogen concentration.

The wedge fiber sensor shown in Figure 10d was studied in more depth by Villatoro et al. [75]. Their studies included multi- and single-mode wedge fibers [76,77], as well as nanoparticle wedge fiber. They fabricated single-mode wedge fiber sensors with a film thickness of 12 nm and an interaction length of 1.5 cm. The variation in optical transmittance versus H_2 concentration was measured for wedge sensors with different tapers using Ar carrier gas, with a sample gas varying from 1.8 to 10% concentration. They found that this sensor does not change the polarization characteristics of the transmitted light. They also investigated the single-mode wedge fiber dispersion effect and found that the transmitted light dispersion effect was significant for light wavelengths in the 900–1600 nm range. The experimental results of Villatoro et al. also showed that although the sensitivity of the multi-mode wedge fiber sensor was lower than that of the single-mode fiber, the stability and ease of use of the multi-mode fiber sensor were much better. They also fabricated multiple multimode wedge fiber sensors with a film thickness of 15 nm, an interaction length of 1 cm, and a wedge fiber girdle diameter between 30 μm and 70 μm. The light source was a LED lamp with a power of 20 μw and a wavelength of 850 nm, and the light transmission rate of the wedge sensors with different tapers was obtained as a function of concentration by measuring the Ar carrier gas with a sample gas in the concentration variation range of 0.3–3.5%. It was found that the sensor transmission intensity increased with the hydrogenation of Pd; however, the light signal saturated after the concentration exceeded a certain value. The response time was 30 s and the recovery time was 90 s at a concentration of 2%; after repeated use of the sensor, the response time and

recovery time were 40 s and 100 s, respectively, and the response time and recovery time increased after multiple uses compared with the first use. The researchers also fabricated a nanoparticle wedge fiber with a film thickness of 4 nm, an interaction length of 2 mm, and a waist spot diameter of 1300 nm. The optical transmittance was measured as a function of concentration using a semiconductor laser with a wavelength of 1550 nm and an Ar carrier gas with a concentration range of 0.8 to 5.2% of the sample gas. In contrast to several other types of sensors, the light intensity of the nanoparticle sensor decreases with increasing hydrogen concentration. The advantage of wedge-shaped fiber-optic sensors is the short waist interaction length and sensitive sensing; however, at the same time, due to the special structure, it is easy to cause waste breakage [78,79].

In 2007, Luna-Moreno et al. [80] developed a structured fiber optic-sensor based on the light wave abruptness effect, which has high stability and sensitivity. They used small segments of single-mode fiber in the length range of 3–8 mm and coated the fiber surface with a Pd film and a Pd alloy film with a film thickness of 10 nm. This thickly coated single-mode fiber segment was then sandwiched between two multi-mode fibers (as shown in Figure 10b). Since the diameter of the single-mode fiber core is smaller than that of the multi-mode fiber core, light can be introduced into the cladding of the single-mode fiber, and the light from the single-mode fiber cladding can be coupled to the sensing film layer. They experimented with Ar carrier gas, which was a sample gas with a concentration range of 0.8 to 4.6%. The results showed that the intensity of transmitted light increased with increasing H_2 concentration. In the same year, Kim et al. [81] also developed a new sensor. They embedded a section of optical fiber into a quartz groove with a radius of curvature of 50 cm and then polished the exposed surface of the fiber embedded in the groove to a remaining thickness of 22 μm. Next, the polished surface was coated with three Pd films with film thicknesses of 20 nm, 40 nm, and 100 nm, respectively, and an interaction length of 2.46 mm. To reduce the effect of polarization during fiber transmission, the fiber's test light wavelength was 1550 nm, and the response and recovery times of the sensor were measured to be 100 s and 150 s, respectively, using an Ar carrier gas with a concentration range between 1 and 2% of the sample gas. Barmenkov [82] reported a fiber laser with intracavity hydrogen sensing. He placed the sensing site of a wedge-shaped fiber sensor into the resonant cavity of an Er-doped fiber laser. Due to the Pd-interaction, the fiber absorption coefficient and the laser cavity loss both decrease, resulting in a lower threshold and a reduced pulse accumulation time. Therefore, the hydrogen concentration can be measured through measuring the pulse accumulation time width.

5.3. Wavelength Modulated Fiber-Optic Sensors

A Bragg grating fiber of a given structure has a certain characteristic wavelength. When a sensor made of Bragg fiber is placed in an H_2 environment, the grating structure changes due to Pd-H_2 interaction, resulting in a shift in the Bragg wavelength, which, in turn, indicates the concentration of hydrogen gas to be measured.

In 1999, Sutapun et al. [83] developed a Bragg grating fiber sensor. They used a single-mode grating fiber with a core of 5–10 μm, a diameter of 125 μm, and a Bragg wavelength of 829.7 nm. Before coating, they etched the cladding of the fiber, and the remaining thickness of the cladding was 35 μm. Figure 12 shows the structure and test results of the grating fiber sensor, with the top panel showing the sensor structure, the middle panel showing the refractive index distribution and the bottom panel showing the transmission and reflection spectral response; Figure 12b also shows the wavelength versus concentration response curve. Due to the Bragg grating written in the optical fiber, the refractive index of the fiber changes periodically, and both transmitted and reflected light are selected for wavelength when the broad-spectrum beam is transmitted. Upon placing the sensor in a hydrogen environment, the fiber stretches, and both the grating constant and refractive index change due to the Pd-H_2 interaction, resulting in a shift in the Bragg wavelength. Experiments were performed with an inert carrier gas, i.e., a sample gas with H_2 concentration variations ranging from 0.3 to 1.8%. Unfortunately, the wavelength drift due to fiber stretching in their

experiments was so small (less than 0.1 nm) that, even with a high-resolution spectrometer (resolution 0.14 nm), it could not be resolved. Thus, they instead used simulations for estimation. They also found that when the measured concentration was 1.8%, there was peeling of the Pd film, which affected the reuse of the sensor. For this reason, they proposed the method of plating a solidifying film between the Pd film and the substrate to solve the film-shedding problem.

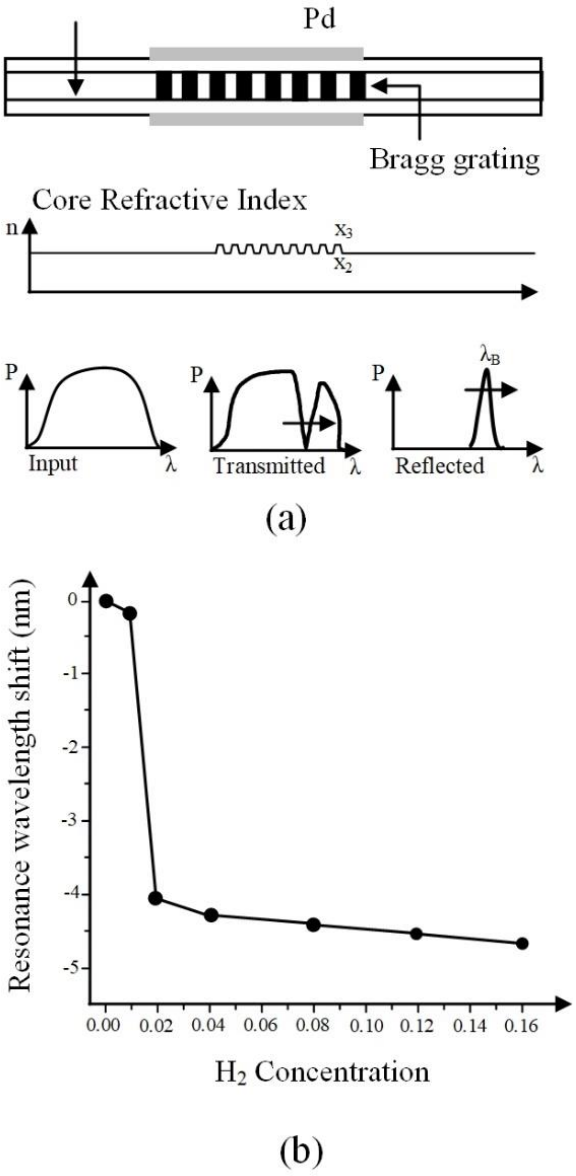

Figure 12. Bragg grating fiber-optic sensor. (**a**) Structure. (**b**) Variation of characteristic wavelength with concentration.

Sutapun originally designed the grating fiber sensor with only the choice of transmitted light wavelength in mind. Later studies found that hydrogenation caused the grating constant to change. However, the choice of wavelength for the sensor is not just limited to the change in the grating constant of the fiber core. The way the transmitted light is coupled to the photoconductor depends on multiple interfaces, including the core/cladding layer, the cladding layer/Pd, and the Pd/outer gas layer, all of which affect the amount of transmitted light wavelength drift. Using the coupling of multiple interfaces, a larger wavelength drift can be achieved. Based on this principle, in 2006, Wei X et al. [84] developed a grating fiber sensor with a large wavelength drift using long-period instead of short-period

grating. This sensor still used a single-mode fiber with a 28 μm core, and a Pd film with a thickness of 50 nm was coated on the outer surface of the cladding via sputtering, with nanoscale particles on the film surface. They measured the variation in wavelength shift versus hydrogen concentration at various temperatures with an inert carrier gas. The wavelength shift of the new sensor was more than two orders of magnitude greater compared to the Sutapun-type sensor. In 2008, Tien et al. [85] used a Bragg single-mode fiber with a core of 10 μm and a diameter of 125 μm. The optical grating period was 0.534 μm, the length was 20 mm, and the characteristic wavelength was 1545 nm. One side of the fiber was polished, and the polished side was coated with a palladium film with a thickness of 20 nm and an interaction length of 12 mm. Experiments were performed with H_2 concentrations varying from 20 to 70% of the sample gas. The experimental results show that the Bragg wavelength increases with increasing hydrogen concentration, and the wavelength drift is large. Maier et al. [86] used a Pd slot with a semicircular cross-section and placed an optical fiber written with a Bragg grating inside the Pd slot, which was coaxial with the Pd slot, and the fiber was fastened to the Pd slot. When the sensor was placed in a hydrogen environment, the Pd tank expanded. The expansion of the Pd tank coupled to the fiber, causing a change in the grating constant. Since the Pd slot expansion had a cumulative effect along the axial direction, it could play an amplifying role in the strain. To ensure the stability of the sensor, the researchers concluded that the thickness of the fabricated Pd slot should not be less than 300 μm.

6. Comparison and Development Trend of Each Sensor

The number of research papers published on different types of hydrogen sensors from 2000 to 2021 (data from Web of Science) is shown in Figure 13, which shows that the interest in and research on hydrogen sensors increased in the past 20 years. The number of articles on semiconductor and fiber-optic sensors is significantly higher than those on catalytic and thermal sensors, which shows that the future research direction and focus will be on semiconductor- and fiber-optic-type hydrogen sensors.

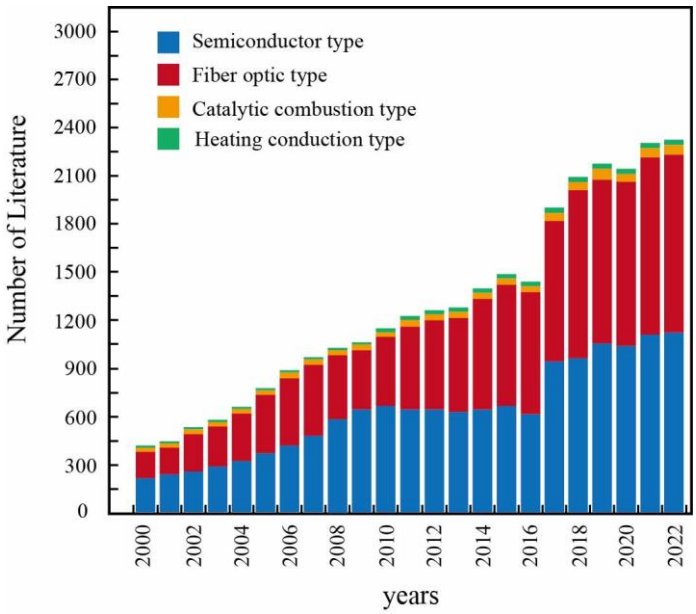

Figure 13. Various sensor research trends since 2000.

Table 1 screens some of the better-performing hydrogen sensors mentioned in the literature. For different types of hydrogen sensors, the focus of current research is slightly different. For example, for catalytic sensors, the power consumption and operating temperature of the sensor are considered, while thermal conductivity sensors usually evaluate the signal-to-noise ratio, output current, and voltage, as well as the effect of temperature

and humidity; fiber-optic sensors focus more on sensitivity and signal demodulation. In terms of response time, the catalytic element- and micromirror-type sensors usually take less than 10 s to respond, while the response time of semiconductor-type sensors is usually less than 30 s, and the response times of grating-, interferometric-, and thermoelectric-type sensors are mostly around 1 min or even longer. Since different unit systems are used to measure the sensitivity of different types of sensors, the lower detection limit is used for comparison in this paper. The lower detection limits of semiconductor-type hydrogen sensors are significantly better than other types, reaching below 10 ppm; the lower detection limits of catalytic- and fiber-optic-type hydrogen sensors are mostly in the range of several hundred ppm. The sensitivity of the sensor is affected by the measurement range, ambient temperature, humidity, the type and thickness of the sensitive material, etc. Changes in temperature and humidity can affect the sensitivity of the sensor to varying degrees. The sensitivity of fiber-optic hydrogen sensors and interferometric sensors is relatively high, reaching more than 10 nm/%; however, these two sensors are susceptible to interference from the measurement environment. The sensitivity of the grating type is relatively low, being generally below 3 nm/%; however, it is easy to compensate for temperature and humidity and realize distributed measurements for industrial applications. Therefore, recent research on grating-type hydrogen sensors focused on developing new sensitive materials and grating structures to improve their sensitivity and avoid their shortcomings. Most of the micro-mirror sensors are scattered light intensity modulated, and most of the literature does not give specific sensitivity values; thus, the sensitivity values of these two sensors are not given in Table 1. The advantage of the micromirror sensor is its simple structure and fast response; however, its structural limitations prevent it from achieving distributed measurements.

Table 1. Comparison of various hydrogen sensors.

Device	Sensitive Materials	[H_2] Range (ppm)	Minimal Detection Limit (ppm)	Response Time (s)	References
Catalytic combustion	TiO_2/Pd/Pt	5000–50,000	/	10	[87]
Catalytic combustion	Pt	20–20,000	/	0.36	[88]
Thermoelectricity	Pt	500–30,000	<500	60	[89]
Thermoelectricity	Pt	500–10,000	250	40	[90]
Semiconductor Type	Pd/GaO_X/GaN	5–10,000	5	22	[91]
Semiconductor Type	Pt/NiO_2	30–1000	30	10	[92]
Fiber-optic microscope	Pd	10,000–100,000	/	<5	[93]
Fiber-optic microscope	Pt/WO_3	0–40,000	/	5	[94]
Fiber-optic grating	110 nm Pd/WO_3	0–90,000	/	<90	[95]
Fiber-optic grating	110 nm Pd/Ni	0–40,000	/	240–300	[96]
Fiber-optic interference	M-Z Pt/WO_3	0–40,000	/	120	[97]
Fiber-optic interference	Sagnac Pt/WO_3	0–10,000	/	60	[98]

In summary, catalytic-type hydrogen sensors have simple structures and fast response times; however, they have high operating temperatures, mostly over 100 °C, which can be a safety hazard, and are cross-sensitive to some gases, such as methane, while oxygen must be present in the environment for use. Thermally conductive hydrogen sensors have long service lives and do not suffer from degradation of device performance due to contamination. However, their selectivity and sensitivity to hydrogen are lower than electrochemical- and semiconductor-type hydrogen sensors. Semiconductor-type hydrogen sensors are simple in structure, small in size, easy to integrate, low in cost, fast in response, and suitable for mass production and use; however, they are affected by electromagnetic interference and prone to signal drift, making them difficult to use in harsher environmental conditions. Fiber-optic sensors have the lowest sensitivity to temperature and humidity, and are more suitable for hydrogen detection in harsh environments, such as high temperature/high humidity, intrinsically safe, resistant to electromagnetic interference, and easy to realize distributed measurement; however, they have long response times, low lower detection

limits, and complicated signal processing at the later stage, as well as a lack of a mature signal demodulation and detection system.

7. Summary and Prospect

At present, the technology behind hydrogen sensors at room temperature is more mature, while the research on sensitivity, response time, safety, lifetime, and other performance factors is also sufficient to meet the needs of the industry. With the continuous development of hydrogen energy in fuel cells, distributed power generation, and human spaceflight, the research on hydrogen sensors, as the core components of the future hydrogen energy-based Internet of Things (IoT), will gradually move towards miniaturization, integration, and distributed sensing, while also focusing on the need to achieve stable measurement in harsh environments, such as high temperature and high humidity. Future research will focus on the following four points:

(1) Reducing the cross-sensitivity of temperature, humidity, and other interference factors, as well as achieving accurate measurement of hydrogen in different environments, is required. The response signal of most hydrogen sensors is affected by temperature and humidity, resulting in cross-sensitivity. Some reducing gases are also absorbed by the hydrogen-sensitive material, which affects hydrogen detection. The cross-sensitivity of the sensor can be reduced via temperature and humidity compensation and surface modification of the hydrogen-sensitive material. The temperature and humidity compensation of the sensor mainly uses hardware and software compensation methods. Hardware compensation includes the bridge arm parallel resistance method, the bridge arm thermistor compensation method, the series-parallel thermistor compensation method outside the bridge, etc. Hardware compensation is usually based on the test data of the sensor in high- and low-temperature environments, and the corresponding temperature compensation components are selected to compensate for the initial zero point and output sensitivity drift of the sensor. Common software compensation methods include interpolation, least squares fitting, BP neural network algorithm, etc. Software compensation is based on the real-time ambient temperature collected via the temperature measurement element, the sensor's zero point, sensitivity, etc., and the temperature change algorithm is integrated into the high-speed computing microcontroller to achieve real-time temperature compensation of the sensor. The use of hardware correction cannot be a complex algorithm compensation, and the compensation circuit is also susceptible to the influence of an electromagnetic environment. In contrast, the software compensation method has high accuracy, a wide range of applications, and simple debugging, and can, therefore, become a common method of sensor temperature compensation.

(2) To develop new hydrogen-sensitive materials, the defects of common hydrogen-sensitive materials, such as Pd and WO_3, can be improved by introducing nanotechnology and adding new materials, such as graphene. The research on hydrogen-sensitive materials never stopped, and the selection of hydrogen-sensitive materials plays a decisive role in the performance of sensors in terms of sensitivity, measurement range, operating temperature, and lifetime. With the development of material science, more new materials will be applied to hydrogen-sensitive materials to improve sensor performance. New hydrogen-sensitive materials, including nanomaterials, hybrid materials, new carbon materials, two-dimensional materials, and metal-organic framework materials, are studied to improve their selectivity and shorten the response time; their sensing materials are gradually developed from traditional metal oxides, such as SnO_2, ZnO, and Fe_2O_3, in the early stage to new metal oxides, such as WO_3, MoO_3, and In_2O_3. Among them, WO_3, as an n-type semiconductor, has a wide range of applications in hydrogen sensing. However, it is difficult for WO_3 monolithic materials to have the characteristics of fast response, low detection limit, and wide detection domain at the same time, and it is necessary to prepare composite materials via physical mixing, loading, and doping, thus enhancing their hydrogen-sensing

performance. The future goal can be to develop hydrogen-sensitive materials with fast response, long-term stability, and good selectivity. Currently, Pd alloys are used to reduce the response time and increase the stability of hydrogen sensors. In addition, magnesium–titanium (Mg-Ti) and magnesium–titanium–nickel (Mg-Ti-Ni) alloy composite films are made into sensors with good repeatability and stability. However, little research was previously performed regarding the selectivity of hydrogen sensors. Moreover, regardless of the measurement method used, the response time is still quite long (tens of seconds and, in some cases, even several minutes or hours); therefore, further research on new sensitive materials is needed.

(3) Research on the applicability of hydrogen sensors at high temperatures is required. The current commercially available several hydrogen sensors have narrow operating temperature ranges, can only be measured at room temperature, and require higher accuracy and lifetimes in high-temperature environments compared to room temperature; thus, the optimization of signal processing and packaging technology should be one of the directions of future research. For example, the performance of fiber-optic hydrogen sensors at high temperatures can be improved by adjusting the internal structure and external packaging of the fiber.

(4) Studying the signal detection and demodulation technology of fiber-optic sensors is also required. The excellent performance of fiber-optic hydrogen sensors facilitates temperature compensation and distributed multi-parameter measurement, which is conducive to the research and development of intelligent sensing systems in the context of the Internet of Things, while it also poses new challenges to the signal detection and demodulation technology of fiber-optic sensors. Currently, the price of a single-channel grating demodulator is over 10,000, and the price of a multi-channel grating demodulator and spectrum analyzer is even higher, which limits the commercialization of fiber-optic hydrogen sensors. Therefore, the development and optimization of software and hardware systems for signal detection and demodulation will be the focus of future research.

Author Contributions: Conceptualization, L.Z. and Y.M.; methodology, G.H.; formal analysis, L.L.; investigation, W.W.; writing—original draft preparation, C.J.; writing—review and editing, Y.Y.; All authors have read and agreed to the published version of the manuscript.

Funding: This research received no external funding.

Institutional Review Board Statement: Not applicable.

Informed Consent Statement: Not applicable.

Data Availability Statement: Data will be made available on request.

Conflicts of Interest: The authors declare no conflict of interest.

References

1. Litvinov, A.; Etrekova, M.; Podlepetsky, B.; Samotaev, N.; Oblov, K.; Afanasyev, A.; Ilyin, V. MOSFE-Capacitor Silicon Carbide-Based Hydrogen Gas Sensors. *Sensors* **2023**, *23*, 3760. [CrossRef] [PubMed]
2. Wu, C.M.; Motora, K.G.; Chen, G.Y.; Kuo, D.H.; Gultom, N.S. Highly efficient reduced tungsten oxide-based hydrogen gas sensor at room temperature. *Mater. Sci. Eng. B* **2023**, *289*, 116285.
3. Nguyen, V.C.; Cha, H.Y.; Kim, H. High Selectivity Hydrogen Gas Sensor Based on WO_3/Pd-AlGaN/GaN HEMTs. *Sensors* **2023**, *23*, 3465. [CrossRef] [PubMed]
4. Lupan, C.; Mishra, A.K.; Wolff, N.; Drewes, J.; Krüger, H.; Vahl, A.; Lupan, O.; Pauporté, T.; Viana, B.; Kienle, L.; et al. Nanosensors Based on a Single ZnO: Eu Nanowire for Hydrogen Gas Sensing. *ACS Appl. Mater. Interfaces* **2022**, *14*, 41196–41207. [CrossRef] [PubMed]
5. Harumoto, T.; Fujiki, H.; Shi, J.; Nakamura, Y. Extremely simple structure hydrogen gas sensor based on single metallic thin-wire under sweep heating. *Int. J. Hydrogen Energy* **2022**, *47*, 34291–34298. [CrossRef]
6. Kim, N.; Cho, H.H.; Kim, Y.; Hwang, J.; Choi, J.Y.; Yu, H.K. Formation of palladium nano-gap on self-cracked WO_3 for hydrogen gas sensors. *Int. J. Hydrogen Energy* **2023**, *48*, 1234–1239. [CrossRef]

7. Okazaki, S.; Kawada, H.; Koshiba, Y.; Kasai, N.; Maru, Y.; Mizutani, T.; Takesaki, Y.; Shimano, S. Catalytic combustion type optical fiber Bragg grating hydrogen gas sensor using platinum-loaded fumed silica powder. *Int. J. Hydrogen Energy* **2023**, *48*, 9512–9527. [CrossRef]
8. Takeo, H. Development of advanced gas-sensing devices based on the microstructural and compositional controls of various promising materials and their different operating mechanism. *J. Ceram. Soc. Jpn.* **2022**, *130*, 739–751.
9. Sarkar, B.; Ratnakar, R.R.; Balakotaiah, V. Bifurcation analysis of catalytically assisted hydrogen combustion in monolith reactors. *Chem. Eng. J.* **2021**, *425*, 130318. [CrossRef]
10. Lan, Y.; Zou, Y.; Ma, X.; Shi, Y.; Fan, J.; Hai, Y.; Wang, X.L.; Yang, J.J.; Feng, Q.H. Fabrication and Characterization of Dual Coordinate Self Examined Thermal Flow Sensor Arrays Based on Longitudinal Heat Conduction. *IEEE Sens. J.* **2020**, *20*, 434–440. [CrossRef]
11. Watanabe, M.; Inoue, R.; Ichikawa, D.; Furusaki, K. Development of Thermal Conductivity Type Hydrogen Sensor. *ECS Trans.* **2020**, *28*, 20.
12. Occelli, C.; Fiorido, T.; Pellegrino, C.P.; Seguin, J.L. Sensors for anaerobic hydrogen measurement: A comparative study between a resistive PdAu based sensor and a commercial thermal conductivity sensor. *Int. J. Hydrogen Energy* **2023**, *48*, 17729–17741. [CrossRef]
13. Kimura, Y.; Ibano, K.; Uehata, K.; Hirai, I.; Lee, T.H.; Ueda, Y. Improved hydrogen gas sensing performance of WO_3 films with fibrous nanostructured surface. *Appl. Surf. Sci.* **2020**, *532*, 147274. [CrossRef]
14. Itoh, T.; Izu, N.; Tsuruta, A.; Akamatsu, T.; Shin, W.; Kamihoriuchi, K.; Takizawa, M.; Yoshida, I. Effect of Pt electrodes in cerium oxide semiconductor-type oxygen sensors evaluated using alternating current. *Sens. Actuators B Chem.* **2021**, *345*, 130396. [CrossRef]
15. Thathsara, S.K.T.; Harrison, C.J.; Hocking, R.K.; Shafiei, M. Photoactive semiconducting metal oxides: Hydrogen gas sensing mechanisms. *Int. J. Hydrogen Energy* **2022**, *47*, 18208–18227. [CrossRef]
16. Liu, H.; Wu, B.; Chen, C.; Zhao, B.L.; Zhang, X.; Zhang, H.C. D-Shaped Tellurite Photonic Crystal Fiber Hydrogen and Methane Sensor Based on Four-Wave Mixing with SPR Effect. *Photonic Sens.* **2023**, *13*, 230121. [CrossRef]
17. Dai, J.; Ruan, H.; Zhou, Y.; Yin, K.; Hu, X.Y.; Ye, Z.; Wang, X.W.; Yang, M.H.; He, P.; Yang, H. Ultra-High Sensitive Fiber Optic Hydrogen Sensor in Air. *J. Light. Technol.* **2022**, *40*, 6583–6589. [CrossRef]
18. Tan, A.J.Y.; Ng, S.M.; Stoddart, P.R.; Hong, S.C. Trends and Applications of U-Shaped Fiber Optic Sensors: A Review. *IEEE Sens. J.* **2021**, *21*, 120–131. [CrossRef]
19. Kabirov, V.A.; Semenov, V.D.; Torgaeva, D.S.; Otto, A.I. Miniaturization of spacecraft electrical power systems with solar-hydrogen power supply system. *Int. J. Hydrogen Energy* **2023**, *48*, 9057–9070. [CrossRef]
20. Kulkarni, P.; Aliprantis, D.; Wu, N.; Loop, B. State Estimation in Spacecraft Power Distribution Systems Using Compound Current Sensors. *IEEE Sens. J.* **2022**, *22*, 23033–23041. [CrossRef]
21. Frei, H.; Burri, M.; Rems, F.; Risse, E.A. A robust navigation filter fusing delayed measurements from multiple sensors and its application to spacecraft rendezvous. *Adv. Space Res.* **2022**. [CrossRef]
22. Choo, T.F.; Saidin, N.U.; Zali, N.M.; Kok, K.Y. Hydrogen and humidity sensing characteristics of Nafion, Nafion/graphene, and Nafion/carbon nanotube resistivity sensors. *J. Nanopart. Res.* **2022**, *24*, 152. [CrossRef]
23. Dai, Y.; Jiang, H.; Zhao, X.; Tian, J.; Deng, X.W.; Zhang, W.L. A temperature-stable Pd nanofilm hydrogen sensor with a Wheatstone bridge structure. *J. Mater. Sci. Mater. Electron* **2023**, *34*, 833.
24. Firth, J.G.; Jones, A.; Jones, T.A. The principles of the detection of flammable atmospheres by catalytic devices. *Combust. Flame* **1973**, *20*, 303–311. [CrossRef]
25. Baker, A. Improvements in or Relating to Electrically Beatable Filaments. UK 892530, 9 August 1959.
26. Houlet, L.F.; Shin, W.; Tajima, K.; Nishibori, M.; Izu, N.; Itoh, T.; Matsubara, I. Thermo-pile sensor-devices for the catalytic detection of hydrogen gas. *Sens. Actuators B Chem.* **2008**, *130*, 200–206. [CrossRef]
27. Krebs, P.; Grisel, A. A low power integrated catalytic gas sensor. *Sens. Actuators B Chem.* **1993**, *13*, 155–158. [CrossRef]
28. Kim, I.J.; Han, S.D.; Han, C.; Gwak, J.; Hong, D.U.; Jakhar, D.; Singh, K.C.; Wang, J.S. Development of micro hydrogen gas sensor with SnO_2-Ag_2O-PtOx composite using MEMS process. *Sens. Actuators B Chem.* **2007**, *127*, 441–446. [CrossRef]
29. Henriquez, D.D.O.; Cho, I.; Yang, H.; Choi, J.; Kang, M.; Chang, K.S.; Jeong, C.B.; Han, S.W.; Park, I. Pt nanostructures fabricated by local Hydrothermal Synthesis for Low-Power Catalytic-Combustion Hydrogen Sensors. *ACS Appl. Nano Mater.* **2021**, *4*, 7–12. [CrossRef]
30. Ivanov, I.I.; Baranov, A.M.; Talipov, V.A.; Mironov, S.M.; Akbari, S.; Kolesnik, I.V.; Orlova, E.D.; Napolskii, K.S. Investigation of catalytic hydrogen sensors with platinum group catalysts. *Sens. Actuator B-Chem.* **2021**, *346*, 130515. [CrossRef]
31. Pranti, A.S.; Loof, D.; Kunz, S.; Zielasek, V.; Bäumer, M.; Lang, W. Design and fabrication challenges of a highly sensitive thermoelectric-based hydrogen gas sensor. *Micromachines* **2019**, *10*, 650. [CrossRef]
32. Hwang, T.Y.; Go, G.M.; Park, S.; Lee, J.; Song, Y.; Kim, S.; Cho, H.B.; Choa, Y.H. Pt/graphene catalyst and tellurium nanowire-based thermochemical hydrogen (TCH) sensor operating at room temperature in wet air. *ACS Appl. Mater. Interfaces* **2019**, *11*, 47015–47024. [CrossRef]
33. Pujadó, M.P.; Gordillo, J.M.S.; Avireddy, H.; Cabot, A.; Morata, A.; Tarancón, A. Highly sensitive self-powered H_2 sensor based on nanostructured thermoelectric silicon fabrics. *Adv. Mater. Technol.* **2020**, *6*, 2000870. [CrossRef]

34. Wang, J.; Liu, Y.; Zhou, H.; Wang, Y.; Wu, M.; Huang, G.; Li, T. Thermal Conductivity Gas Sensor with Enhanced Flow-Rate Independence. *Sensors* **2022**, *22*, 1308.
35. Xu, K.; Liao, N.B.; Xue, W.; Zhou, H.M. First principles investigation on MoO_3 as room temperature and high temperature hydrogen gas sensor. *Int. J. Hydrogen Energy* **2020**, *45*, 9252–9259. [CrossRef]
36. Kaaliveetil, S.; Yang, J.; Alssaidy, S.; Li, Z.L.; Cheng, Y.H.; Menon, N.H.; Chande, C.; Basuray, S. Microfluidic Gas Sensors: Detection Principle and Applications. *Micromachines* **2022**, *13*, 1716. [CrossRef]
37. Hopper, R.; Popa, D.; Udrea, F.; Ali, S.Z.; Marbell, P.S. Miniaturized thermal acoustic gas sensor based on a CMOS microhotplate and MEMS microphone. *Sci. Rep.* **2022**, *12*, 1690. [CrossRef]
38. Yang, G.; Zhang, Z.; Zhang, Y.L.; Luo, Y.Y.; Xiong, X.; Duan, G.T. Thermal simulation of micro hotplate for multiple MEMS gas sensors. *Chin. J. Anal. Chem.* **2022**, *50*, 38–43. [CrossRef]
39. Matsumiya, M.; Shin, W.; Qiu, F.; Izu, N.; Matsubara, I.; Murayama, N. Poisoning of platinum thin film catalyst by hexamethyldisiloxane (HMDS) for thermoelectric hydrogen gas sensor. *Sens. Actuators B Chem.* **2003**, *99*, 309–315. [CrossRef]
40. Choi, Y.; Tajima, K.; Shin, W.; Izu, N.; Matsubara, I.; Murayama, N. Combustor of ceramic Pt/alumina catalyst and its application for micro-thermoelectric hydrogen sensor. *Appl. Catal. A Gen.* **2005**, *287*, 19–24. [CrossRef]
41. Shin, W.; Matsumiya, M.; Qiu, F.; Izu, N.; Murayamaet, N. Thermoelectric gas sensor for detection of high hydrogen concentration. *Sens. Actuator B Chem.* **2004**, *97*, 344–347. [CrossRef]
42. Qiu, F.; Shin, W.; Matsumiya, M.; Izu, N.; Matsubara, I.; Murayama, N. Miniaturization of thermoelectric hydrogen sensor prepared on glass substrate with low-temperature crystallized SiGe film. *Sens. Actuators B Chem.* **2004**, *103*, 252–259. [CrossRef]
43. Tian, J.W.; Jiang, H.C.; Deng, X.W.; Zhang, L.Y.; Zhang, J.F.; Zhao, X.H.; Zhang, W. Zero drift suppression for PdNi nano-film hydrogen sensor by vacuum annealing. *Int. J. Hydrogen Energy* **2020**, *45*, 14594–14601. [CrossRef]
44. Liu, Y.; Li, Y.L. Signal analysis and processing method of transmission optical fiber hydrogen sensors with multi-layer Pd–Y alloy films. *Int. J. Hydrogen Energy* **2019**, *44*, 27151–27158. [CrossRef]
45. Almaev, A.V.; Kopyev, V.V.; Novikov, V.A.; Chikiryaka, A.V.; Yakovlev, N.N.; Usseinov, A.B.; Karipbayev, Z.T.; Akilbekov, A.T.; Koishybayeva, Z.K.; Popov, A.I. ITO Thin Films for Low-Resistance Gas Sensors. *Materials* **2023**, *16*, 342. [CrossRef] [PubMed]
46. Maho, P.; Herrier, C.; Livache, T.; Comon, P.; Barthelme, S. A calibrant-free drift compensation method for gas sensor arrays. *Chemom. Intell. Lab. Syst.* **2022**, *225*, 104549.
47. Chiu, S.W.; Tang, K.T. Towards a chemiresistive sensor integrated electronic nose: A review. *Sensors* **2013**, *13*, 14214–14247. [CrossRef]
48. Rashid, T.R.; Phan, D.T.; Chung, G.S. A flexible hydrogen sensor based on Pd nanoparticles decorated ZnO nanorods grown on polyimide tape. *Sens. Actuators B Chem.* **2013**, *185*, 777–784. [CrossRef]
49. Mirzaei, A.; Yousefi, H.R.; Falsafi, F.; Bonyani, M.; Lee, J.H.; Kim, J.H.; Kim, H.W.; Kim, S.S. An overview on how Pd on resistive-based nanomaterial gas sensors can enhance response toward hydrogen gas. *Int. J. Hydrogen Energy* **2019**, *44*, 20552–20571. [CrossRef]
50. Singh, G.; Singh, R.C. Highly sensitive gas sensor based on Erdoped SnO_2 nanostructures and its temperature dependent selectivity towards hydrogen and ethanol. *Sens. Actuators B Chem.* **2019**, *282*, 373–383. [CrossRef]
51. Wang, T.T.; Ma, S.Y.; Cheng, L.; Luo, J.; Jiang, X.H.; Jin, W.X. Preparation of Yb-doped SnO_2 hollow nanofibers with an enhanced ethanol-gas sensing performance by electrospinning. *Sens. Actuators B Chem.* **2015**, *216*, 212–220. [CrossRef]
52. Gottam, S.R.; Tsai, C.T.; Wang, L.W.; Wang, C.T.; Lin, C.C.; Chu, S.Y. Highly sensitive hydrogen gas sensor based on a MoS_2-Pt nanoparticle composite. *Appl. Surf. Sci.* **2020**, *506*, 144981. [CrossRef]
53. Hermawan, A.; Asakura, Y.; Kobayashi, M.; Kakihana, M.; Yin, S. High temperature hydrogen gas sensing property of GaN prepared from α-GaOOH. *Sens. Actuators B Chem.* **2018**, *276*, 388–396. [CrossRef]
54. Hermawan, A.; Asakura, Y.; Yin, S. Morphology control of aluminum nitride (AlN) for a novel high-temperature hydrogen sensor. *Int. J. Min. Met. Mater.* **2020**, *27*, 1560–1567. [CrossRef]
55. Ajayan, J.; Nirmal, D.; Ramesh, R.; Bhattacharya, S.; Tayal, S.; Joseph, L.M.I.L.; Thoutam, L.R.; Ajitha, D. A critical review of AlGaN/GaN-heterostructure based Schottky diode/HEMT hydrogen (H_2) sensors for aerospace and industrial applications. *Measurement* **2021**, *186*, 110100. [CrossRef]
56. Irokawa, Y. Hydrogen sensors using nitride-based semiconductor diodes: The role of metal/semiconductor interfaces. *Sensors* **2011**, *11*, 674–695. [CrossRef]
57. Baik, K.H.; Jang, S. AlGaN/GaN heterostructure based hydrogen sensor with temperature compensation. *ECS J. Solid. State Sci. Technol.* **2020**, *9*, 045010. [CrossRef]
58. Zhao, Y.; Shen, J.C.; Liu, Q.; Zhu, C.L. Optical fiber sensor based on helical Fibers: A review. *Measurement* **2022**, *188*, 110400. [CrossRef]
59. Sun, Y.Z.; Yan, Z.J.; Zhou, K.M.; Luo, B.B.; Jiang, B.Q.; Mou, C.B.; Sun, Q.Z.; Zhang, L. Excessively Tilted Fiber Grating Sensors. *J. Light. Technol.* **2022**, *39*, 3761–3770.
60. Ran, Z.; He, X.; Rao, Y.; Sun, D.; Qin, X.J.; Zeng, D.B.; Chu, W.W.; Li, X.K.; Wei, Y.B. Fiber-Optic Microstructure Sensors: A Review. *Photonic Sens.* **2021**, *11*, 227–261. [CrossRef]
61. Wang, Y.; Mumtaz, F.; Dai, Y. Hydrogen gas sensor based on seven-core fiber interference and Pt-WO_3 film. *Mater. Lett.* **2023**, *341*, 134245. [CrossRef]
62. Butler, M.A. Optical fiber hydrogen sensor. *Appl. Phys. Lett.* **1984**, *45*, 1007–1009. [CrossRef]

63. Butler, M.A.; Ginley, D.S. Hydrogen sensing with palladium-coated optical fibers. *J. Appl. Phys.* **1988**, *64*, 3706–3712. [CrossRef]
64. Han, S.; Chen, Y.; Gang, Z.; Liu, Y.; Huang, P.C.; Zhao, H.W.; Yang, M.H.; Dai, J.X.; Li, Z. Optical fiber hydrogen sensor based on an annealing-stimulated Pd–Y thin film. *Sens. Actuators B Chem.* **2015**, *216*, 11–16.
65. Jackson, D.A.; Priest, R.; Dandridge, A.; Tveten, A.B. Elimination of drift in a single-mode optical fiber interferometer using a piezoelectrically stretched coiled fiber. *Appl. Opt.* **1980**, *19*, 2926–2929. [CrossRef]
66. Butler, M.A. Fiber Optic Sensor for Hydrogen Concentrations near the Explosive Limit. *J. Electrochem. Soc.* **1991**, *138*, 236–251. [CrossRef]
67. Butler, M.A. Micromirror optical-fiber hydrogen sensor. *Sens. Actuators Chem.* **1994**, *22*, 155–163. [CrossRef]
68. Butler, M.A.; Buss, R.J. *Kinetics of the Micromirror Chemical Sensor*; Elsevier: Amsterdam, The Netherlands, 1993; Volume 11, pp. 161–166.
69. Kalli, K.; Othonos, A.; Christofides, C. Characterization of reflectivity inversion, α- and β-phase transitions and nanostructure formation in hydrogen activated thin Pd films on silicon based substrates. *J. Appl. Phys.* **2002**, *91*, 3829–3840. [CrossRef]
70. Armgarth, M.; Nylander, C. Blister formation in Pd gate MIS hydrogen sensors. *IEEE Electron Device Lett.* **1983**, *3*, 384–386. [CrossRef]
71. Matelon, R.J.; Avila, J.I.; Volkmann, U.G.; Cabrera, A.L.; Morales, E.H.; Lederman, D. Substrate effect on the optical response of thin palladium films exposed to hydrogen gas. *Thin Solid Film.* **2008**, *516*, 7797–7801. [CrossRef]
72. Borgschulte, A.; Gremaud, R.; Man, S.D.; Westerwaal, R.J.; Rector, J.H.; Dam, B.; Griessen, R. High-throughput concept for tailoring switchable mirrors. *Appl. Surf. Sci.* **2006**, *253*, 1417–1423. [CrossRef]
73. Dam, B.; Gremaud, R.; Broedersz, C.; Griessen, R. Combinatorial thin film methods for the search of new lightweight metal hydrides. *Scr. Mater.* **2007**, *56*, 853–858. [CrossRef]
74. Tabib-azar, M.; Sutapub, B.; Petrick, R.; Kazemi, A.A. Highly sensitive hydrogen sensors using palladium coated fiber optics with exposed cores and evanescent field interactions. *Sens. Actuators B Chem.* **1999**, *56*, 158–163. [CrossRef]
75. Villatoro, J.; Luna-moreno, D.; Monzón-Hernández, D. Optical fiber hydrogen sensor for concentrations below the lower explosive limit. *Sens. Actuators B Chem.* **2005**, *110*, 110–117. [CrossRef]
76. Villatoro, J.; Díez, A.; Cruz, J.L.; Andreés, M.V. Highly sensitive optical hydrogen sensor using circular Pd-coated singlemode tapered fibre. *Electron. Lett.* **2001**, *37*, 1011–1012. [CrossRef]
77. Villatoro, J.; Díez, A.; Cruz, J.L.; Andres, M.V. In-line highly sensitive hydrogen sensor based on palladium-coated single-mode tapered fibers. *IEEE Sens. J.* **2003**, *3*, 533–537. [CrossRef]
78. Joel, V.; David, M.-H. Fast detection of hydrogen with nano fiber tapers coated with ultra thin palladium layers. *Opt. Express* **2005**, *13*, 5087.
79. Zalvidea, D.; Diez, A.; Cruz, J.L.; Andres, M.V. Wavelength multiplexed hydrogen sensor based on palladium-coated fibre-taper and Bragg grating. *Electron. Lett.* **2004**, *40*, 301–302. [CrossRef]
80. Luna-moreno, D.; Monzón-hernández, D. Effect of the Pd–Au thin film thickness uniformity on the performance of an optical fiber hydrogen sensor. *Appl. Surf. Sci.* **2007**, *253*, 8615–8619. [CrossRef]
81. Kim, K.T.; Song, H.S.; Mah, J.P.; Hong, K.B.; Im, K.; Baik, S.J.; Yoon, Y.I. Hydrogen sensor based on palladium coated side-polished single-mode fiber. *IEEE Sens. J.* **2007**, *7*, 1767–1771. [CrossRef]
82. Kazemi, A.A.; Goswami, K.; Mendoza, E.A. Time-domain fiber laser hydrogen sensor. *Opt. Lett.* **2004**, *29*, 2461–2463.
83. Sutapun, B.; Tabib-azar, M.; Kazemi, A. Pd-coated elastooptic fiber optic Bragg grating sensors for multiplexed hydrogen sensing. *Sens. Actuators B Chem.* **1999**, *60*, 27–34. [CrossRef]
84. Wei, X.; Wei, T.; Xiao, H.; Lin, Y.S. Nano-structured Pd-long period fiber gratings integrated optical sensor for hydrogen detection. *Sens. Actuators B Chem.* **2008**, *134*, 687–693. [CrossRef]
85. Tien, C.L.; Chen, H.W.; Liu, W.F.; Jyu, S.S.; Lin, S.W.; Lin, Y.S. Hydrogen sensor based on side-polished fiber Bragg gratings coated with thin palladium film. *Thin Solid Film.* **2008**, *516*, 5360–5363. [CrossRef]
86. Maier, R.R.J.; Jones, B.J.S.; Barton, J.S.; Mcculloch, S.; Jones, B.J.S.; Burnell, G. Fibre optics in palladium-based hydrogen-sensing. *J. Opt.* **2007**, *9*, S45–S49. [CrossRef]
87. Han, C.H.; Hong, D.W.; Han, S.D.; Gwak, J.; Singh, K.C. Catalytic combustion type hydrogen gas sensor using TiO_2 and UV-LED. *Sens. Actuator B* **2007**, *125*, 225–228. [CrossRef]
88. Lee, E.B.; Hwang, I.S.; Cha, J.H.; Lee, H.J.; Lee, W.B.; Pak, J.J.; Lee, J.H.; Ju, B.K. Micromachined catalytic combustible hydrogen gas sensor. *Sens. Actuator B Chem.* **2011**, *153*, 392–397. [CrossRef]
89. Shin, W.; Matsumiya, M.; Izu, N.; Murayama, N. Hydrogen-selective thermoelectric gas sensor. *Sens. Actuator B Chem.* **2003**, *93*, 304–308. [CrossRef]
90. Sabah, F.A.; Ahmed, N.M.; Hassan, Z.; Rasheed, H.S. High performance CuS p-type thin film as a hydrogen gas sensor. *Sens. Actuator A Phy.* **2016**, *249*, 68–76. [CrossRef]
91. Liu, I.P.; Chang, C.H.; Lu, H.H.; Lin, K.W. Hydrogen sensing performance of a GaN-based Schottky diode with an H_2O_2 treatment and electroless plating approach. *Sens. Actuator B Chem.* **2019**, *296*, 126599. [CrossRef]
92. Chen, W.P.; Xiong, Y.; Li, Y.S.; Cui, P.; Guo, S.S.; Chen, W.; Tang, Z.L.; Yan, Z.J.; Zhang, Z.Y. Extraordinary room-temperature hydrogen sensing capabilities of porous bulk Pt-TiO_2 nanocomposite ceramics. *Int. J. Hydrogen Energy* **2016**, *41*, 3307–3312. [CrossRef]

93. Bevenot, X.; Trouillet, A.; Veillas, C.; Gagnaire, H.; Clement, M. Hydrogen leak detection using an optical fibre sensor for aerospace applications. *Sens. Actuator B-Chem.* **2000**, *67*, 57–67. [CrossRef]
94. Xu, B.; Chang, R.; Li, P.; Wang, D.N.; Zhao, C.L.; Li, J.Q.; Yang, M.H.; Duan, L.Z. Reflective optical fiber sensor based on light polarization modulation for hydrogen sensing. *J. Opt. Soc. Am. B* **2019**, *36*, 3471–3478. [CrossRef]
95. Dai, J.; Yang, M.; Chen, Y.; Cao, K.; Liao, H.; Zhang, P.C. Side-polished fiber Bragg grating hydrogen sensor with WO_3-Pd composite film as sensing materials. *Opt. Express* **2011**, *19*, 6141–6148. [CrossRef]
96. Dai, J.; Yang, M.; Yu, X.; Cao, K.; Liao, J.S. Greatly etched fiber Bragg grating hydrogen sensor with Pd/Ni composite film as sensing material. *Sens. Actuator B Chem.* **2012**, *174*, 253–257. [CrossRef]
97. Hu, T.Y.; Wang, D.N.; Wang, M.; Li, Z.; Yang, M.H. Miniature hydrogen sensor based on fiber inner cavity and Pt-doped WO_3 coating. *IEEE Photon Technol. Lett.* **2014**, *26*, 1458–1461. [CrossRef]
98. Xu, B.; Zhao, C.L.; Yang, F.; Gong, H.P.; Wang, D.N.; Dai, J.X.; Yang, M.H. Sagnac interferometer hydrogen sensor based on panda fiber with Pt-loaded WO_3/SiO_2 coating. *Opt. Lett.* **2016**, *41*, 1594–1597. [CrossRef]

Disclaimer/Publisher's Note: The statements, opinions and data contained in all publications are solely those of the individual author(s) and contributor(s) and not of MDPI and/or the editor(s). MDPI and/or the editor(s) disclaim responsibility for any injury to people or property resulting from any ideas, methods, instructions or products referred to in the content.